

THESIS FOR THE DEGREE OF DOCTOR OF PHILOSOPHY

Structural Requirements for Selective DNA Binding

Studies on Mono- and Binuclear Ruthenium Complexes

JOHANNA ANDERSSON



Department of Chemical and Biological Engineering

CHALMERS UNIVERSITY OF TECHNOLOGY

Gothenburg, Sweden 2012

Structural Requirements for Selective DNA Binding - Studies on Mono- and Binuclear
Ruthenium Complexes
JOHANNA ANDERSSON
ISBN 978-91-7385-632-4

© JOHANNA ANDERSSON, 2012.

Doktorsavhandlingar vid Chalmers tekniska högskola
Ny serie nr 3313
ISSN 0346-718X

Department of Chemical and Biological Engineering
Chalmers University of Technology
SE-412 96 Gothenburg
Sweden
Telephone + 46 (0)31-772 1000

Printed by Chalmers Reproservice
Gothenburg, Sweden 2012

Structural Requirements for Selective DNA Binding – Studies on Mono- and Binuclear Ruthenium Complexes

JOHANNA ANDERSSON

Department of Chemical and Biological Engineering
Chalmers University of Technology

ABSTRACT

Ever since the discovery of the role of DNA as the template for protein synthesis, efforts have been made to develop DNA targeted drugs. One of the major challenges in the design of DNA binding drugs is to achieve selective binding to specific DNA sequences, which is crucial to avoid side effects. In this thesis, the relationship between molecular structure and DNA binding properties for a group of ruthenium complexes is investigated with focus on sequence selectivity and binding affinity. In particular, threading intercalation, an unusual DNA binding mode sometimes observed for dumbbell shaped molecules, is examined. The study is motivated by the fact that threading intercalating binuclear ruthenium complexes previously have been shown to bind selectively to long stretches of AT-base pairs, which potentially can be used to target parasites with high AT-content in their genomes. The dissociation from DNA is also very slow, which is a property thought to be important for biological activity.

In this thesis, it is demonstrated by spectroscopic DNA binding studies on four new binuclear complexes that threading intercalating ability is very sensitive to bridging ligand structure. The presence of a dppz-moiety is important for threading to occur and increased flexibility is not beneficial for this type of binding. Shortening of the bridging ligand increases the AT-selectivity but reduces the binding constant. Further, it is demonstrated that the enantioselectivity is different for the two DNA grooves. A new mononuclear threading intercalating complex with aryl substituents on the dppz-ligand is presented, for which it is shown that reduced complex charge can be compensated for by structural variations to maintain slow dissociation. Altogether, three new threading intercalators have been developed. From calorimetric studies on non-threading mononuclear complexes it is evident that cooperativity effects have large influence on binding to AT-DNA. Those effects are probably present also for threading intercalating binuclear complexes and may explain some of the observations made for such complexes. Finally, cell studies show that threading intercalation is possible also in the intracellular milieu and that binuclear complexes are internalized in live CHO-K1 cells, though endosomal escape may be a potential problem for biological applications.

KEYWORDS: ruthenium, DNA, threading intercalation, sequence selectivity, enantioselectivity, kinetics, spectroscopy, cell studies, calorimetry

LIST OF PUBLICATIONS

This thesis is based on the work presented in the following papers:

- I. **AT-Specific DNA Binding of Binuclear Ruthenium Complexes at the Border of Threading Intercalation**
Johanna Andersson, Minna Li and Per Lincoln*
Chemistry – a European Journal **2010**, 16, 11037–11046
- II. **Stereoselectivity for DNA Threading Intercalation of Short Binuclear Ruthenium Complexes**
Johanna Andersson and Per Lincoln*
Journal of Physical Chemistry B **2011**, 115, 14768–14775
- III. **Slow Threading Intercalation of Monomeric Ru(II) Complexes with 10,13-Diarylsubstituted dppz Ligands**
Minna Li, Per Lincoln, and Johanna Andersson*
Journal of Physical Chemistry B **2011**, 115, 7923–7931
- IV. **Ligand-Ligand Interactions in DNA Binding – a Calorimetric Study of Ru-dppz Enantiomers**
Johanna Andersson, Louise Fornander, Maria Abrahamsson, Eimer Tuite, Pär Nordell and Per Lincoln*
Manuscript
- V. **Effects of Chirality on the Intracellular Localization of Binuclear Ruthenium(II) Polypyridyl Complexes**
Frida R. Svensson, Johanna Andersson, Helene L. Åmand, and Per Lincoln*
Journal of Biological Inorganic Chemistry **2012**,
DOI: 10.1007/s00775-012-0877-0

Related publications not included in this thesis:

Photoswitched DNA-Binding of a Photochromic Spiropyran

Johanna Andersson, Shiming Li, Per Lincoln, and Joakim Andréasson*

Journal of the American Chemical Society **2008**, *130*, 11836–11837

Molecular AND-logic for Dually Controlled Activation of a DNA-binding Spiropyran

Martin Hammarson, Johanna Andersson, Shiming Li, Per Lincoln and Joakim Andréasson*

Chemical Communications **2010**, *46*, 7130–7132

CONTRIBUTION REPORT

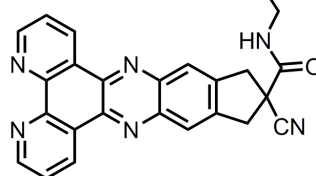
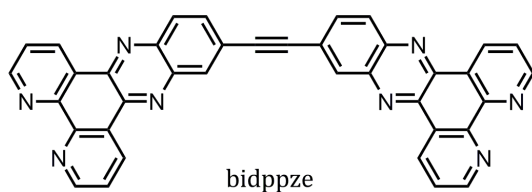
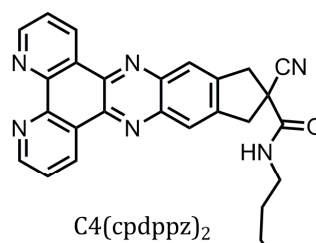
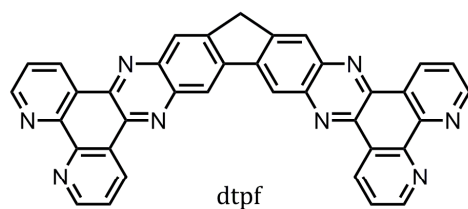
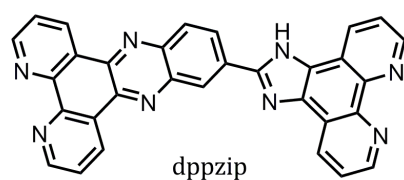
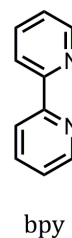
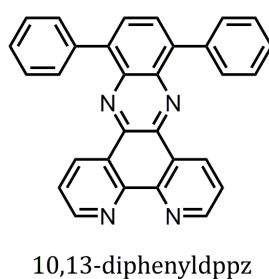
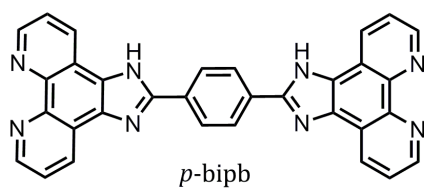
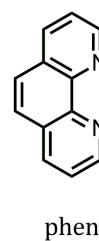
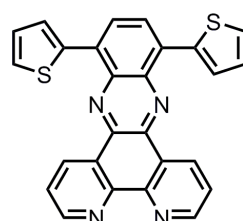
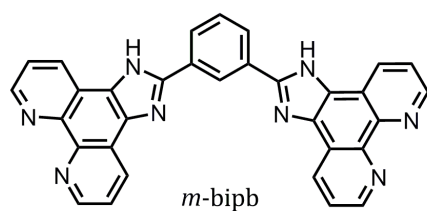
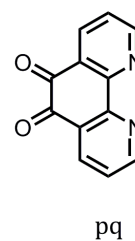
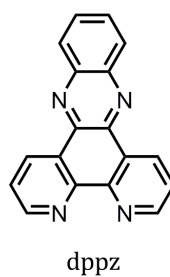
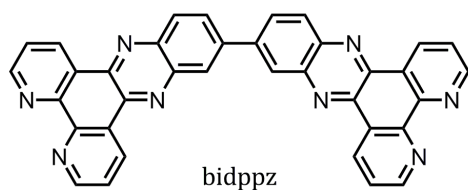
- Paper I: This paper is mainly my work. Minna Li developed the synthetic route for complex 3.
- Paper II: This paper is mainly my work.
- Paper III: I performed part of the DNA binding studies, analyzed the data and wrote the paper. The synthetic work was done by Minna Li. The Matlab program was developed by Per Lincoln.
- Paper IV: I did part of the experimental work, contributed in planning the experiments and developing the binding model, did main part of the data analysis and wrote part of the paper. Matlab programs were developed by Per Lincoln.
- Paper V: I contributed in planning the study and analyzing the data. I wrote main part of the paper. The experimental work was performed by Frida Svensson.

The previously unpublished results presented here are mainly my work except the cell experiments which were performed by Frida Svensson and the synthesis of complex 4 which was done by Johan Johansson. Yubo Wang performed part of the DNA binding studies on complex 4 under my supervision.

LIGAND ABBREVIATIONS

<i>m</i> -bipb	1,3-bis(imidazo[4,5-f]1,10-phenanthroline-2-yl)benzene
<i>p</i> -bipb	1,4-bis(imidazo[4,5-f]1,10-phenanthroline-2-yl)benzene
bidppz	11,11'-bis(dipyrido[3,2-a:2',3'-c]phenazinyl)
bidppze	bis(dipyrido[3,2-a:2',3'-c]phenazin-11-yl)ethyne
bpy	2,2'-bipyridine
C4(cpdppz) ₂	N,N'-bis(12-cyano-12,13-dihydro-11H-cyclopenta[b]dipyrido[3,2-h:2',3'-j]phenazine-12-carbonyl)-1,4-diaminobutane
dppz	dipyrido[3,2-a:2',3'-c]phenazine
dppzip	2-(dipyrido[3,2-a:2',3'-c]phenazin-11-yl)imidazo[4,5-f]1,10-phenanthroline
dtpf	4,5,9,12,16,17,21,25-octaaza-23H-ditriphenylene[2,3-b:2',3'-h]-fluorene
phen	1,10-phenanthroline
pq	1,10-phenanthroline-5,6-dione

LIGAND STRUCTURES



CONTENTS

1	INTRODUCTION	1
2	BACKGROUND	3
2.1	Structure and Function of Nucleic Acids.....	3
2.2	DNA as a Drug Target.....	6
2.3	Threading Intercalation.....	7
2.4	Why Ruthenium Complexes?.....	8
3	FUNDAMENTAL CONCEPTS AND METHODOLOGY	11
3.1	Synthesis of Enantiopure Ruthenium Complexes.....	11
3.2	Absorption and Emission of Light.....	12
3.3	Photophysical Properties of Ruthenium Polypyridyl Complexes.....	14
3.4	Probing DNA Binding by Emission Spectroscopy.....	15
3.5	Determining Binding Geometry by Linear Dichroism.....	17
3.6	Studying DNA Binding by Circular Dichroism.....	20
3.7	Kinetic Characterization of Threading Intercalation.....	20
3.8	Binding Thermodynamics and Isothermal Titration Calorimetry.....	22
3.9	Binding Isotherms and the McGhee-von Hippel Model.....	24
3.10	Studying Cell Interactions by Confocal Microscopy.....	25
4	RESULTS	27
4.1	Bridging Ligand Structure.....	27
4.2	Enantioselectivity and Enantiomeric Preferences of the Grooves.....	31
4.3	A New Substitution Pattern for Threading Intercalating dppz Complexes.....	35
4.4	Thermodynamics and Cooperativity for Intercalating dppz Complexes.....	37
4.5	Cell Localization and Uptake.....	42
5	CONCLUDING REMARKS	45
6	ACKNOWLEDGEMENTS	49
7	REFERENCES	51

1 INTRODUCTION

All living species, from small bacteria and parasites to higher order organisms such as humans, share one common thing: they all consist of cells. Cells are membrane enclosed self-replicating entities, which lodge a complex machinery of macromolecules that every day performs billions of chemical reactions in order to maintain the well-being of the organism. One of the main components in the cell is deoxyribonucleic acid, DNA, which stores the genetic information and serves as a template for protein production. The DNA molecule is a long chain of four different building blocks, the nucleobases adenine, thymine, guanine and cytosine. The order of the bases along the DNA chain constitutes the genetic code, where each combination of three consecutive bases corresponds to a specific amino acid, the amino acids being the units building up the proteins. Hence, the order of bases in the genome determines the order of amino acids in the proteins, and as a consequence, errors in the sequence of nucleobases may result in erroneous proteins. As the proteins are responsible for the majority of the vital functions in the cell, such as signaling, regulation, transportation, catalysis, structure and movement, malfunctioning proteins may cause severe damage to the cells which may lead to diseases or even death of the organism.

Proteins, both human and bacterial, are the main drug targets in the search for new therapeutical agents. This is due to their crucial role in the cell machinery, but also the fact that the activity of many proteins can specifically be either enhanced or suppressed by binding of small synthetic molecules to them.¹ The discovery of the role of DNA as a template for protein synthesis has increased the interest for DNA as a potential drug target.²⁻³ Instead of trying to alter the activity of already existing proteins, the idea is to regulate the production of them by binding of small molecules to the protein encoding genes. The genome sequencing projects have enabled assignment of genes and regulatory sequences in both human DNA⁴ as well as the genomes of other organisms, thus providing insight regarding what DNA sequences that might be interesting to target. However, this information is of little use as long as the mechanisms behind specific DNA binding are poorly understood. Although the double helical structure of DNA was proposed by Watson and Crick already in 1953,⁵ and the DNA molecule itself as well as DNA binding drugs have been extensively studied since, the problem to achieve sequence specific binding still remains as one of the major challenges in the development of DNA targeting drugs.

Threading intercalation is an unusual DNA binding mode, in which part of the drug molecule has to be threaded through the base pair stack for binding to occur.⁶⁻⁸ This results in extremely slow kinetics for the interaction as well as the binding being selective towards flexible DNA structures such as long stretches of AT-base pairs.⁹ Consequently, threading intercalating compounds are interesting as model compounds for DNA targeting drugs, and a better understanding of the mechanisms behind this type of binding mode would be valuable for future design of new drugs with slow dissociation and improved sequence selectivity. In this thesis, the DNA binding properties of several different ruthenium complexes are investigated. The aim is to elucidate how threading intercalation ability and selectivity is affected, and hopefully can be controlled, by structural variations of the compounds. The studies may also lead to insights regarding how different types of DNA behave in the interaction with drug molecules. Finally, results from cell studies on binuclear ruthenium complexes are discussed in an attempt to evaluate the biological relevance of the DNA binding studies and the potential use of binuclear ruthenium complexes for biomedical applications.

In the following chapters, a more detailed background to the work as well as a brief description of the experimental methods and some fundamental concepts will be given, before the main results are presented.

2 BACKGROUND

The main theme in this thesis is interactions between synthetic molecules and DNA, with special attention on the DNA binding mode threading intercalation. This chapter aims to explain how and why DNA can be exploited as a drug target and gives an introduction to the most fundamental aspects of drug-DNA interactions. The main characteristics of threading intercalation are also described and the choice of ruthenium complexes as model compounds for this type of DNA interaction is motivated.

2.1 Structure and Function of Nucleic Acids

Deoxyribonucleic acid (DNA) is a double stranded, right-handed helical structure, where the two strands are polymers built up from four different units, the nucleotides. Each nucleotide consists of phosphoric acid esterified with a deoxyribose sugar that forms the repetitive unit of the polymer backbone, and, attached to the deoxyribose group, one of the four bases adenine (A), guanine (G), thymine (T) or cytosine (C) (Figure 2.1). The two-ring bases A and G are commonly referred to as purines, whereas the one-ring bases T and C are known as pyrimidines. In the closely related ribonucleic acid (RNA), which is usually single stranded, the sugar is ribose that carries one extra hydroxyl group compared with deoxyribose, and the methyl group is missing on thymine.^{5, 10}

At physiological pH, the phosphate groups in the backbone of the DNA double helix are negatively charged while the surface of the base pairs is quite hydrophobic. As a result of the hydrophobic effect, the base pairs stack on top of each other with the bases pointing towards the center of the helix and the backbone positioned on the outside facing the surrounding water. In addition to the hydrophobic effect, the two strands of the double helix are held together by hydrogen bonds between the bases, where A always pairs with T, and G with C. This specific hydrogen bonding pattern, also referred to as base pairing, results in the two strands being complementary to each other, and accounts for the storage and replication of the genetic information. As seen in Figure 2.1, only two hydrogen bonds are formed between A and T compared with three for G and C, resulting in the AT-base pairs being less stable, and thus more flexible, than the GC-base pairs. Although RNA mainly exists as single stranded molecules, the strands often folds into three-dimensional structures with duplex regions where base pairing occurs. RNA can also base pair with single stranded DNA, which is of great importance for the production of proteins as described below.^{5, 10}

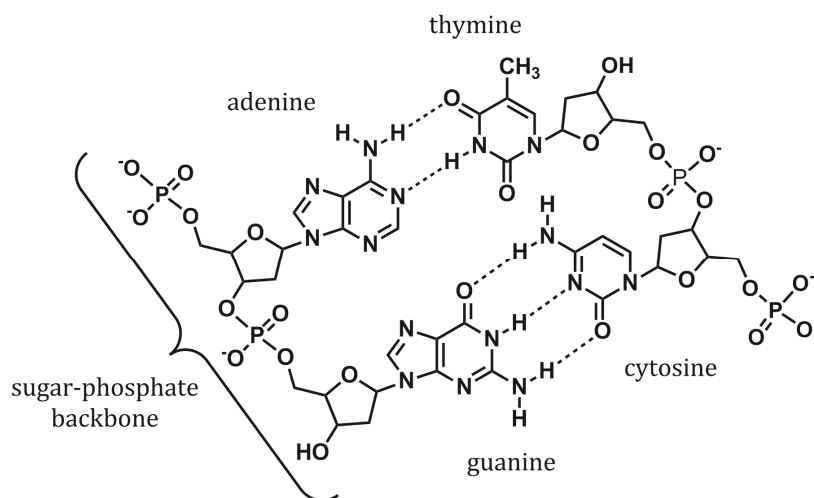


Figure 2.1. Structure of the nucleotides and the sugar-phosphate backbone in a dinucleotide duplex.

Double helical nucleic acids can exist in three different conformations: A-, B- and Z-form (Figure 2.2). All three forms are found in biological systems, though for DNA the B-form is by far the most abundant. Between the backbones of the two strands there are two grooves, one on each side of the base pair stack, which in the B-form have equal depths but different widths; the major groove, as the name implies, being wider than the minor groove. In A-DNA the bases are somewhat displaced from the center of the helix and the base pairs are inclined at a large angle relative the helix axis, resulting in a deep and narrow major groove and a shallow minor groove. This conformation is mainly observed for double stranded RNA and DNA-RNA duplexes, but also occurs in double stranded DNA at short stretches of sequential purines or as a result of dehydration or protein binding. Z-DNA is a left-handed structure that is observed for long alternating purine-pyrimidine sequences, mainly GC.¹⁰⁻¹¹ In addition to the above mentioned duplex structures, there are regions in the DNA where the duplex structure is perturbed. Hairpins, loops and bulges are all structures that contain unpaired bases, and while they play an important role for RNA structure and function, they mainly arise in natural DNA as a result of mutations on one of the DNA strands.¹⁰

Before cell division occurs, the DNA is duplicated to provide both daughter cells with a complete set of the genetic information, a process referred to as replication. During replication, the two strands of the double helix are separated from each other, and new DNA strands are synthesized along each of the single strands, which act as templates for the synthesis. Nucleotides are added to the growing strands by a protein called polymerase, but only nucleotides that are correctly base paired with a nucleobase on the template strand are incorporated in the growing strand. Hence, the newly synthesized strand will be complementary to

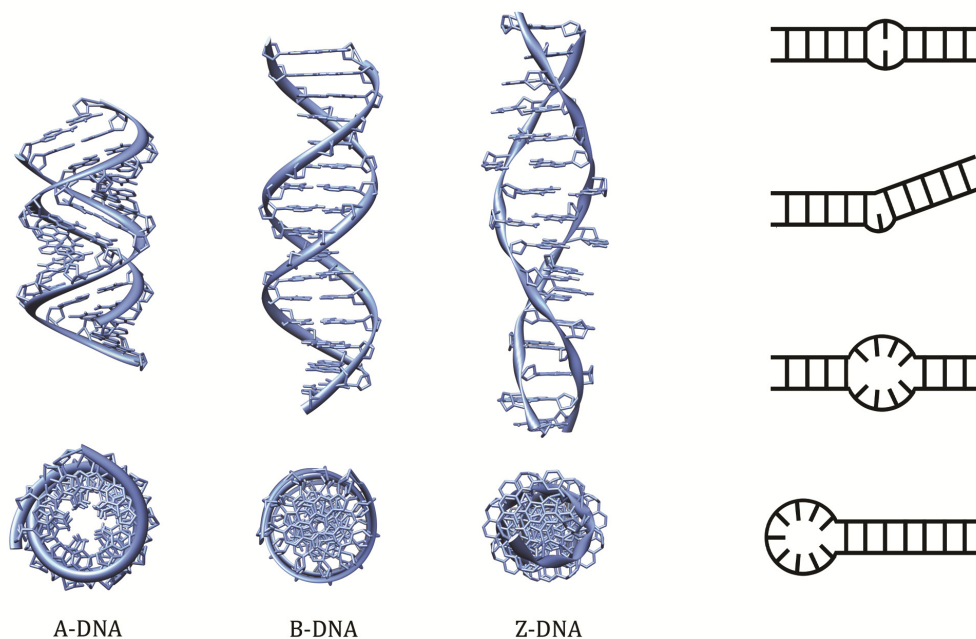


Figure 2.2. Left: A- B- and Z-form of a 16 base pair DNA-duplex, sideview (top) and topview (bottom). Right: schematic picture of non-duplex structures. From top to bottom: mismatch, bulge, internal loop and hairpin loop.

the template strand, and the genetic information will be maintained. The first step in protein synthesis, transcription of the information stored in the gene into messenger RNA, is very similar to replication: the two DNA strands are separated from each other and one of them serves as a template for synthesis of a complementary strand of RNA. The RNA is then translated by the ribosomes into a long chain of amino acids, a polypeptide chain, that folds itself into a three dimensional structure that forms the functional protein. Both replication and transcription requires binding of a number of proteins, such as the polymerase and various transcription factors, to the DNA.¹² If the assembly of the replication/transcription proteins on the DNA is inhibited, e.g. by binding of small drug molecules to the DNA, cell division and protein synthesis can no longer occur. Thus, DNA is interesting as a drug target for diseases where cell proliferation needs to be inhibited, such as cancer or bacterial infections, or diseases caused by protein overproduction.¹³ In theory, it should be possible to also enhance the production of a specific protein if the bound drug attracts the transcription machinery to the DNA, but efforts to mimic transcription factors with small peptide containing synthetic molecules has proven this to be far more difficult.¹⁴

2.2 DNA as a Drug Target

Compared to proteins, where the drug usually binds to a specific motif of hydrogen bonds and hydrophobic patches that is unique to each protein, DNA is a quite uniform structure. The DNA helix does not fold into a three dimensional structure in the same way as the polypeptide chains of proteins do, thus providing few means to distinguish different sequences from each other. Ever since the discovery of the duplex structure by Watson and Crick, efforts have been made to correlate DNA structure with sequence, but with little success because the structural differences between the base pairs are miniscule.¹⁵ The different duplex and non-duplex structures mentioned above may serve as a tool for recognition, but as they are not gene specific they cannot alone act as the recognition pattern for a drug. The most promising strategy to target specific DNA sequences so far, seems to be to exploit the base pair sequence.

Although covalent binding of drugs to the DNA is an excellent way of inhibiting DNA related processes, as seen for example by the successful use of DNA-alkylating anti-cancer drugs,¹⁶⁻¹⁸ covalent interactions are not as efficient when it comes to recognition of specific genes. In order to target a specific gene the drug has to interact with a relatively large fragment of the DNA (13-17 base pairs^{17, 19-20}), and here non-covalent interactions play an important role. In addition to the electrostatic interaction between positively charged ions and the negatively charged DNA, there are two major modes of non-covalent DNA binding: groove binding and intercalation.¹⁰ Groove binding can occur in either of the two grooves, with the major groove being mainly the site for protein binding due to its larger size.¹⁴ Typical synthetic groove binding drugs are small crescent-shaped molecules that interact with the minor groove via hydrogen bonds and van der Waals interactions. Intercalation refers to the insertion of a molecule or part of a molecule, usually a flat heteroaromatic polycyclic ring system, between two adjacent base pairs, where it interacts with the bases by π -stacking.²¹ Generally, groove binding occurs without major distortions of the DNA structure, whereas intercalation results in lengthening and unwinding of the DNA which is associated with a significant cost in free energy that has to be compensated for by superior hydrophobic interactions. It should be noted that many DNA intercalators have side groups that interact with the grooves upon binding, sometimes making it difficult to clearly distinguish between groove binders and intercalators.

The sequence selectivity of DNA intercalators is generally rather poor because the drug only interacts with the two base pairs forming the intercalation pocket and sequence has little influence on the intercalation pocket itself. Groove binders, on the other hand, are much more promising as sequence specific DNA binding drugs as both grooves display a sequence specific pattern of functional groups that can be used for recognition. In the major groove, all four possible combinations of base pairs display different hydrogen bonding capabilities, whereas in the minor groove AT and TA base pairs have identical properties.^{14, 22-23} The perhaps most obvious way to achieve specific binding in the major groove is to use short

oligonucleotides that bind to purines via Hoogsteen base pairing forming triple-helix structures. However, the fact that the target sequence must contain several consecutive purines on the same strand, combined with the chemical instability and poor membrane permeability of oligonucleotides, limit their therapeutical use.^{3, 14, 23} Dervan and co-workers have developed double stranded crescent shaped hairpin polyamides, consisting of pyrrole, hydroxypyrrole and imidazole units connected via peptide bonds, which can recognize all four base pairs from the minor groove by a combination of hydrogen bonds and sterical interactions.²³⁻²⁴ DNA sequences as long as 16 base pairs have been selectively targeted by this method,²⁰ and the polyamides have been shown to inhibit viral replication in human cells by preventing minor groove binding transcription factors to access the DNA.²⁵⁻²⁶ Although this is a very promising strategy to design gene specific DNA binding drugs, it is limited by the fact that the polyamides bind the minor groove while the majority of DNA-protein interactions occur in the major groove.¹⁴ The polyamides can however be used to guide chemotherapeutics of poor selectivity to a specific gene.²⁷

Due to the difficulties to target specific genes, DNA binding drugs are still a rarity among commercially available pharmaceuticals.¹ Only in the treatment of cancer, where the aim is to kill the tumor cells, have DNA binding drugs found widespread use.^{17-18, 28} Anti-cancer drugs generally bind unspecifically to the whole genome, and discrimination between healthy and tumor cells occurs by other mechanisms, such as differences in cellular uptake of the drug.¹⁷⁻¹⁸ The selectivity is still poor, though, and cancer chemotherapy is normally associated with severe side effects. There are examples of DNA binding drugs that display antibacterial, antifungal or antimalarial effects that are/could be of therapeutical use,²⁹ but also for these drugs selectivity occurs on cell rather than gene level. For example, the AT-selective drugs pentamidine, berenil and furamidine are active against diseases caused by protozoan parasites, where one proposed mechanism of action is binding of the drugs to kinetoplasts, i.e. AT-rich circular DNA found in the parasite mitochondria.³⁰⁻³¹

2.3 Threading Intercalation

In addition to the common non-covalent DNA binding modes, intercalation and groove binding, there is a third one termed threading intercalation, which combines intercalation with interactions in the grooves. The typical threading intercalator is a flat heterocyclic aromatic molecule with bulky, and very often also charged, substituents in both ends. As the name implies, one of the bulky substituents has to be threaded through the base pair stack for intercalation of the flat middle part to occur, resulting in the bulky substituents being located in opposite grooves in the bound state (Figure 2.3). The threading process requires large distortions of the DNA structure, in some cases even transient base pair opening,^{8, 32} resulting in both threading and dissociation from the threaded state being extremely slow processes.^{6-7, 33} Several intercalating units can also be

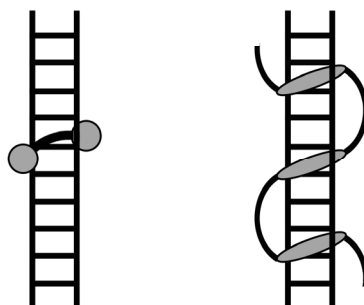


Figure 2.3. Schematic picture of threading intercalation (left) and polyintercalation (right). Both types of binding modes require threading of bulky groups through the base pair stack.

connected via flexible linkers to create poly-intercalators that thread the DNA in order to insert all their intercalating units in the base pair stack.³⁴⁻³⁸

Threading intercalation was first discovered for the natural antibiotic nogalamycin, whose cytotoxic activity was assigned to the slow dissociation from DNA.^{6-8, 39-40} As there appears to be a correlation between slow dissociation kinetics and cytotoxicity,^{7, 41-43} threading intercalating compounds are interesting as potential DNA targeting drugs, and efforts have been made to develop synthetic threading intercalators.^{33, 44-57} Figure 2.4 shows examples of molecules that have been shown to bind DNA by threading intercalation. None of them displays as slow kinetics as nogalamycin, but focus has instead been on targeting specific DNA and RNA structures. Many threading intercalators bind selectively to DNA and RNA bulges and loops since such structures already contain a “loophole” where the bulky substituent more easily can pass through the base pair stack.^{50-53, 58} There are also examples of threading intercalators that target quadruplex structures.⁵⁴⁻⁵⁵ Further, a poly-intercalator containing sequence specific peptide links has been reported to selectively target a 14 bp long DNA fragment with extremely slow dissociation compared with corresponding monomeric threading intercalators.³⁷

2.4 Why Ruthenium Complexes?

Since Barton’s pioneering DNA binding studies on $[\text{Ru}(\text{phen})_3]^{2+}$ in the mid 1980’s,⁵⁹ this and related ruthenium polypyridyl complexes have received considerable interest as probes for DNA, arising from the possibility to synthesize stable complexes where the emission properties can be fine-tuned by varying the ligands.⁶⁰⁻⁶² Over the years, numerous complexes have been designed for this purpose, the perhaps most well-known being the light-switch complexes $[\text{Ru}(\text{phen})_2\text{dppz}]^{2+}$ and $[\text{Ru}(\text{bpy})_2\text{dppz}]^{2+}$, which are completely quenched in aqueous solution but become brightly luminescent upon intercalation into DNA.⁶³⁻⁶⁴ Recently, focus has shifted somewhat to also include more biomedical

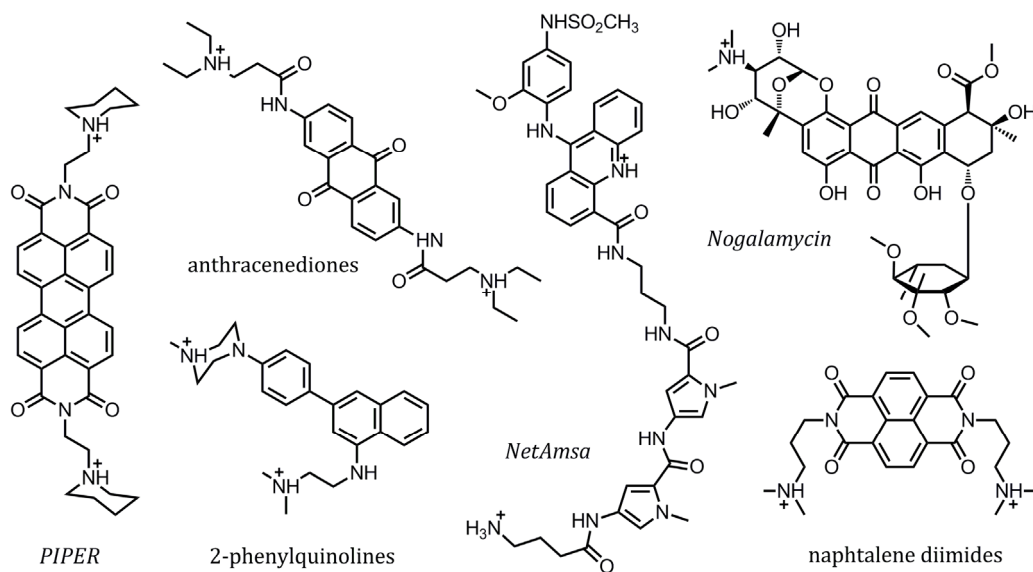


Figure 2.4. Examples of different types of threading intercalators. Compound names are written in *italic* whereas classes of compounds are labeled in *regular font*.

applications. There are examples in the literature of ruthenium complexes that selectively target different DNA and RNA bulge structures,⁶⁵ display cytotoxic activity,⁶⁶⁻⁶⁷ compact DNA,⁶⁸⁻⁶⁹ and stain various cellular components,⁷⁰⁻⁷² with potential use as diagnostic probes, anti-cancer drugs, gene delivery vectors and imaging agents, respectively.

Even if threading bisintercalation of the flexibly linked dimer $[\mu\text{-C4}(\text{cpdppz})_2\text{-}(\text{phen})_4\text{Ru}_2]^{4+}$ was demonstrated 1999,³⁵⁻³⁶ it was quite a surprise when it was serendipitously discovered in 2002 that the binuclear ruthenium complex $[\mu\text{-bidppz}(\text{phen})_4\text{Ru}_2]^{4+}$ binds DNA by threading intercalation.⁷³ The DNA interactions of this complex and its bipyridine homologue have since been intensively studied as these complexes possess a number of properties that make them suitable as a model compounds in the quest for understanding of the mechanisms behind threading intercalation. The kinetics is extremely slow compared with other synthetic threading mono-intercalators, with dissociation rate constants in the same range as those for nogalamycin.^{7, 73} The slow kinetics is important for biological activity as mentioned above, but also enables studies of the initial non-threading interactions with DNA. In combination with the fact that these complexes also exhibit light-switch properties,⁷³ the slow kinetics makes it easy to study the threading process by conventional spectroscopic techniques. Previous studies have mainly been focused on characterization of the threading mechanism and kinetics,⁷⁴⁻⁷⁶ as well as the selectivity for various DNA targets.^{9, 77-78} The latter resulted in the discovery that threading of the complex is kinetically selective towards long (>10 bp) sequences of alternating AT-base pairs,⁷⁸ a property that could potentially be used to target parasites with AT-rich genomes.^{30-31, 79} Finally,

the presence of ruthenium ions facilitates systematic variations of complex structure, which is central to the work in this thesis, where focus is on the complexes rather than the DNA targets. The ruthenium (II) ion has an octahedral coordination geometry, which in combination with slow ligand exchange rates, enables synthesis of stable and enantiomerically pure complexes by coordination of bidentate ligands to the ruthenium. The coordination of ruthenium to polypyridyl ligands is generally strong enough to allow harsh reaction conditions, which is an advantage since the ligands can be chemically modified also when coordinated to the ruthenium.⁶²

3 FUNDAMENTAL CONCEPTS AND METHODOLOGY

The DNA binding properties of several ruthenium complexes have been investigated in this thesis. The DNA binding studies have mainly been focused on evaluating structural effects of the intercalating part on threading intercalation ability and sequence selectivity of the complexes. This has been done by comparison of their association and dissociation rates as well as relative binding constants to [poly(dAdT)]₂ (AT-) and calf thymus(ct)-DNA, using different spectroscopic techniques. Isothermal titration calorimetry has been used to study the thermodynamics of the interactions between mononuclear dppz complexes, the smallest common unit of the threading intercalating complexes, and AT-DNA. Finally, the uptake and distribution in both live and fixed cells has been studied using confocal laser scanning microscopy. Below follows a brief description of the mentioned techniques and some fundamental concepts, aiming to explain how they were used in this project and how to interpret the results in the following chapter.

3.1 Synthesis of Enantiopure Ruthenium Complexes

Coordination of bidentate ligands, such as phenanthroline or bipyridine, to divalent ruthenium results in complexes that exist in two enantiomeric forms, the right-handed Δ -form and the left-handed Λ -form (Figure 3.1). Previous studies have revealed large differences between the enantiomers in their interactions with DNA, and therefore it is important to investigate the complexes in their enantiomerically pure forms. The synthesis of the pure enantiomers of the studied complexes is based on the strategy developed by Lincoln for synthesis of enantiopure [Ru(phen)₂dppz]²⁺, where homochiral [Ru(phen)₂pq]²⁺ is obtained by resolving the racemate into the pure Δ - and Λ -enantiomers by repeated recrystallization with arsenyl D(-)- or L(+)-tartrate, respectively.⁶⁴ Due to the stability of bidentate ruthenium complexes, the pure enantiomers of the diquinone can then be used as starting material for the synthesis of larger enantiopure ruthenium complexes.

Since only imagination and synthetic skills set the limit for how many different ligands can be made, and ligands, chirality around the ruthenium ions, number of ruthenium ions etc. can be combined in a seemingly infinite number of ways, all

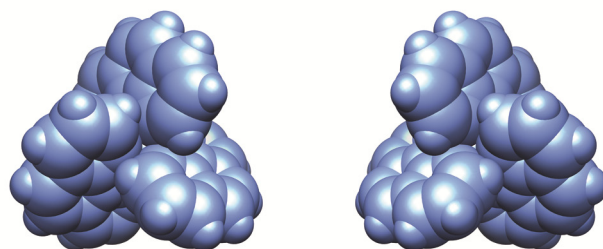


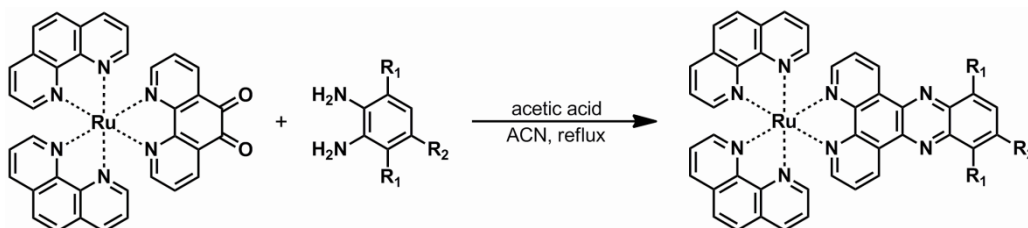
Figure 3.1. The Λ - (left) and Δ -enantiomer (right) of $[\text{Ru}(\text{phen})_3]^{2+}$.

conceivable structures could impossibly be examined. The new complexes have been designed with the well studied $[\mu\text{-bidppz}(\text{phen})_4\text{Ru}_2]^{4+}$ as model where the intercalating part has been systematically varied. Also, it was important that the complexes could be obtained in relatively few reaction steps. Two reactions in particular have been central for the complexes investigated in this thesis: the formation of a phenazine-moiety by reacting the diquinone with an *orto*-diamine (Scheme 3.1) and the formation of an benzimidazole-moiety by reacting the diquinone with an aldehyde using ammonium acetate as nitrogen source (Scheme 3.2). By varying the substituents on the diamine and the aldehyde, all the investigated complexes could be obtained using these reactions.

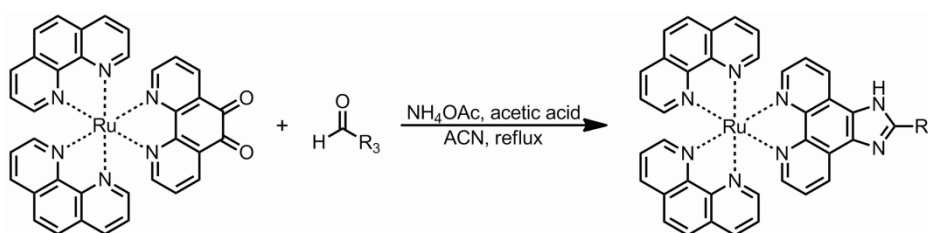
3.2 Absorption and Emission of Light

Molecules can be excited from their ground state to higher electronic states by interaction with light, a process referred to as absorption. In order for absorption to occur, the Bohr frequency condition has to be satisfied, i.e. the energy of the incident light has to exactly match the energy difference between the ground state and the excited state of the absorbing molecule. This is utilized in different spectroscopic techniques where the extent of absorption is measured as a function of wavelength, i.e. the energy of the light. The energy difference between the ground state and the excited state depends not only on the structure of the molecule but also the environment around the chromophore. Therefore spectroscopic techniques can be used to probe DNA binding, as the environment around the chromophore changes when bound to DNA compared with when free in solution.

Light is composed of an electric and a magnetic field oscillating in perpendicular directions relative to each other and to the direction of propagation. In order for absorption to occur, the electric field has to induce an oscillation in the electronic charge distribution of the chromophore. This oscillating charge distribution gives rise to a transition dipole moment, which for each transition has a fixed direction with respect to the molecule structure. The probability for absorption to occur is proportional to the magnitude of the transition dipole moment μ as well as the



Scheme 3.1. Formation of the phenazine-moiety used in the synthesis of complex **3**, **4**, **P** and **T**.



Scheme 3.2. Formation of the benzimidazole-moiety used in the synthesis of complex **2** and **3**.

angle θ between the transition dipole moment and the oscillation direction of the incoming light:⁸⁰

$$A \propto \mu^2 \cos^2 \theta \quad (\text{Equation 3.1})$$

An electronically excited molecule can return to the ground state by both radiative and non-radiative pathways as depicted in the Jablonski diagram (Figure 3.2). In contrast to absorption, which always occurs with conservation of spin, both radiative and non-radiative relaxation processes may involve a change of spin. Internal conversion and intersystem crossing are both non-radiative processes, meaning that no emission of light occurs upon relaxation. Internal conversion does not involve a change of spin and can be described as a conversion of electronic energy into vibrational energy, which is then dissipated as heat to the surroundings. Intersystem crossing, on the other hand, is the conversion of a singlet (spin-paired) excited electronic state to an excited triplet (unpaired) electronic state (or vice versa). Such a transition is formally forbidden according to quantum mechanics and hence very slow, but the rate of this process can be greatly enhanced in presence of a heavy atom due to spin-orbit coupling.

Fluorescence is the process when the system relaxes from an excited singlet state to the ground state with concomitant emission of light. Because internal conversion from higher excited states to the first excited state is much faster (occurs within 10^{-12} s) than emission of light, fluorescence generally occurs from

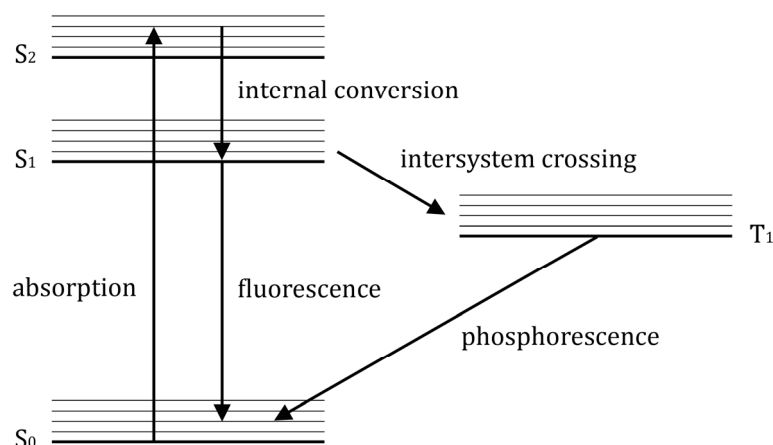


Figure 3.2. Jablonski diagram illustrating the transitions between different electronic states. Solid and dashed arrows indicate radiative and non-radiative processes, respectively.

the lowest vibrational level of the first excited state. The emissive relaxation from an excited triplet state to the ground state is termed phosphorescence. Because it is spin-forbidden it is a slow process that occurs on the timescale of milliseconds to seconds, as compared with nanoseconds for fluorescence, but in resemblance to intersystem crossing the rate can be enhanced by the presence of heavy atoms. The Bohr frequency condition has to be fulfilled also for fluorescence and phosphorescence, and the emitted light can thus be used to probe the environment of the chromophore.⁸¹

3.3 Photophysical Properties of Ruthenium Polypyridyl Complexes

Absorption of light by ruthenium polypyridyl complexes results in a number of different excited singlet states. Most of them arises from intraligand $\pi \rightarrow \pi^*$ transitions or $d \rightarrow \pi^*$ metal-to-ligand charge-transfer (MLCT) transitions, where a ligand π electron or a metal d electron is excited to a ligand π^* orbital, respectively. All those excited states rapidly and efficiently undergo intersystem crossing to a state usually referred to as the lowest energy excited triplet state, a ³MLCT state, the rate and efficiency of this spin-forbidden process being greatly enhanced due to spin-orbit coupling with the ruthenium heavy atom. Relaxation of the ³MLCT state to the singlet ground state via non-radiative pathways is relatively slow. Thus, the excited state is rather long lived, allowing relaxation to the ground state also by emission of light. As emission occurs from what is seen as a triplet state, it would be regarded as phosphorescence. However, the presence of the ruthenium atom results in significant singlet-triplet mixing of the electronic states, which means that the lowest energy excited state also have substantial singlet character. Phosphorescence is therefore not an entirely correct description of the emission

which for example occurs for example on much faster timescales (100 ns - 10 μ s) than what is usually observed for phosphorescence, though it is still slower than fluorescence.⁸¹⁻⁸³

Although ruthenium complexes in general are luminescent, many ruthenium complexes containing a dppz-moiety are non-emissive in water. The complexes are still highly luminescent in non-polar environments, though, and this extreme sensitivity for the surroundings is commonly referred to as the light-switch effect.^{63-64, 84-86} The origin of this phenomenon has been studied in detail for the model compounds $[\text{Ru}(\text{phen})_2\text{dppz}]^{2+}$ and $[\text{Ru}(\text{bpy})_2\text{dppz}]^{2+}$, and it has been concluded that the emissive $^3\text{MLCT}$ state, which is located on the dppz ligand, is effectively quenched in protic solvents by hydrogen bonding to the phenazine nitrogens on the dppz ligand.⁸⁶ Olofsson et al. have shown that the fully quenched species results from hydrogen bonding to both phenazine nitrogens, whereas complexes with one and no hydrogen bonds both are emissive but with different emission lifetimes.⁸⁷ Although addition of substituents to the dppz ligand may alter the photophysical properties of the complex,⁸⁶ the threading intercalating binuclear ruthenium complexes studied in this thesis also exhibit light-switch properties. Thus, when the dppz-moiety of these complexes is intercalated between the DNA base pairs the phenazine nitrogens are protected from water and the complexes become luminescent, which enable studies of the threading process by fluorescence spectroscopy. By contrast, the mononuclear 10,13-diaryl-substituted dppz complexes studied in Paper III are non-luminescent in aqueous solution as well as acetonitrile and when bound to DNA, and can thus not be studied by fluorescence spectroscopy, while the imdazophenanthroline complexes used as cellular probes in Paper V luminesce brightly regardless of solvent.

3.4 Probing DNA Binding by Emission Spectroscopy

When an emissive molecule is excited to a higher electronic state, it will remain in the excited state for a period of time before it relaxes to the ground state. Since emission of light is a random process, the time spent in the excited state varies within a population of excited molecules. Thus, the emission of a population of chromophores, all excited at $t = 0$, is a first order decay process (Equation 3.2) where the emission intensity I_t reflects the fraction of molecules that are still excited at time t after excitation and the emission lifetime τ describes the average time spent in the excited state.

$$I_t = I_0 \exp(-t/\tau) \quad (\text{Equation 3.2})$$

The emission lifetime depends on the rates of both the emissive and non-emissive relaxation processes according to Equation 3.3 where k_r and k_{nr} denote the rate constants for radiative and non-radiative relaxation processes, respectively.

$$\tau = \frac{1}{k_r + k_{nr}} \quad (\text{Equation 3.3})$$

In a population of excited molecules, not all of them will relax by emission of light but some will return to the ground state by non-radiative processes. The fraction of molecules that relaxes via emissive processes depends on the relative size of k_r and k_{nr} . If k_r is larger than k_{nr} , relaxation is more likely to occur by emission of light, and vice versa. The efficiency of the emission, i.e. how many of the absorbed photons that will be emitted as light upon relaxation, is given by the emission quantum yield Φ .⁸¹

$$\Phi = \frac{k_r}{k_r + k_{nr}} \quad (\text{Equation 3.4})$$

While k_r is an intrinsic property of the fluorophore k_{nr} is very sensitive to the environment, and as a consequence both the emission lifetimes and quantum yield can be used to probe the environment of a chromophore. For dppz complexes, where the accessibility of the dppz ligand to hydrogen bonding water is the major factor controlling the emission, these properties reflect the environment of the dppz ligand. A high quantum yield and long emission lifetimes are indicative of efficient protection of the dppz ligand from water, and by comparison of those parameters for different complexes in the presence of DNA conclusions can be made about their relative binding constants and their binding modes. In particular, if there are differences in the emission lifetimes between two DNA bound enantiomers of the same complex, these differences must be due to different binding modes because enantiomers of the same molecule has the same k_r . Further, an estimate of the relative binding constants of two enantiomers can be obtained by comparing their apparent intrinsic emission lifetimes. The intrinsic lifetime τ_0 , which is the inverse of k_r and thus should be the same for enantiomers of the same molecule, can be calculated from the observed emission lifetime and the quantum yield according to:

$$\tau_0 = \frac{\tau}{\Phi} \quad (\text{Equation 3.5})$$

If the calculated intrinsic lifetime differs between the enantiomers, this is an indication that there is a fraction of non-emitting species in the samples, which in the case of dppz complexes probably are complexes that are not intercalated in the DNA. These molecules absorb photons at the excitation wavelength but do not emit any, thus lowering the observed quantum yield resulting in erroneous intrinsic lifetimes. The relative values of the calculated emission lifetimes reflect the relative fractions of non-emitting species in the samples, and thus relative binding constants can be estimated. Finally, the existence of multiple emission lifetimes in a sample containing only one type of fluorophore indicates the presence of several different species of the fluorophore. For dppz complexes, multiple emission lifetimes in presence of DNA are thought to arise from different intercalated species with different accessibility of the dppz ligand to water.⁸⁶

3.5 Determining Binding Geometry by Linear Dichroism

Because absorption is most efficient when the electric field of the incident light is oscillating parallel to the transition dipole moment of the absorbing molecule (Equation 3.1), the absorption of linearly polarized light by a molecule will largely depend on their relative orientations. This phenomenon is utilized in linear dichroism (LD) spectroscopy, where the difference in absorption of light polarized parallel and perpendicular to the reference axis of a macroscopically oriented sample is measured:⁸⁸⁻⁸⁹

$$LD = A_{\parallel} - A_{\perp} \quad (\text{Equation 3.6})$$

There are several available methods to achieve orientation of an LD sample, such as the use of stretched polymers, electric or magnetic field orientation and flow orientation. Here, Couette cell flow orientation, which is suitable for orientation of long polymers such as DNA, has been used.⁹⁰ The Couette cell consists of two concentric quartz cylinders with a narrow spacing in between where the sample is applied. Rotation of one of the cylinders creates a shear flow gradient between the cylinders that causes the long DNA molecules to align in the flow direction (Figure 3.3). The advantage of this method is that only drug molecules bound to the DNA give rise to LD signals since ligand molecules free in solution are too small to be oriented.

From Equation 3.6 it is evident that an LD signal larger than zero indicates that the transition dipole moment giving rise to the signal is oriented more parallel to the reference axis while a negative signal suggests a more perpendicular orientation. By convention, the reference axis for uniaxial samples is defined as the unique axis of the sample. Thus, in the case of flow-oriented DNA the DNA helix axis is chosen as the reference axis, and consequently a negative LD signal means that the transition dipole moment is oriented more perpendicular to the helix axis.⁸⁸⁻⁸⁹

If the polarization directions of the transition dipole moments within the molecule are known, a more quantitative analysis of the LD spectra, and hence the binding geometry, is possible. For each absorption band, the angle α between the transition dipole moment and the reference axis can be calculated from the reduced linear dichroism, LD^r , which is the LD divided by the isotropic absorption, using Equation 3.7.

$$LD^r = \frac{A_{\parallel} - A_{\perp}}{A_{iso}} = \frac{3}{2} S(3\cos^2\alpha - 1) \quad (\text{Equation 3.7})$$

As previously described, the absorption spectra of ruthenium polypyridyl complexes are composed of several different electronic transitions, which overlap each other. In such cases, the determination of the binding geometry becomes a bit complicated since the LD^r of each individual transition dipole moment cannot be directly determined from the experimental LD spectra. However, if the shape of the

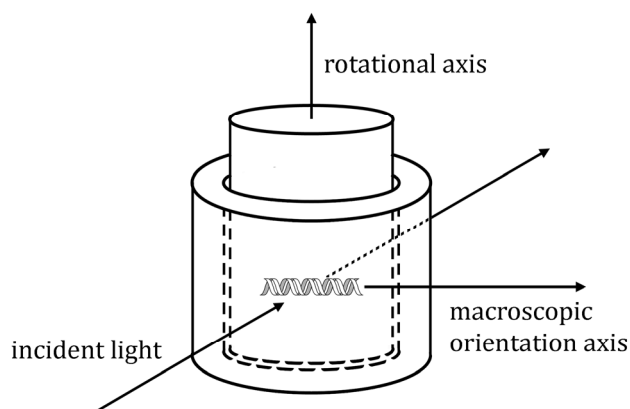


Figure 3.3. Schematic picture of the Couette flow cell. Rotation of the inner cylinder creates a shear flow in which long molecules are aligned.

absorption spectra of each individual transition dipole moment is known, as well as their polarization directions within the molecule, α for all transition dipole moments can be obtained by considering all transitions separately. The isotropic absorption spectra can be seen as a linear combination of the absorption bands of all transition dipole moments. Similarly, the LD spectra can be seen as a weighted sum of the same absorption bands, where the weights are given by the right hand side of Equation 3.7. Thus, if the shapes of the absorption bands are known for all transition dipole moments, the overall absorption and LD spectra can be constructed by summarizing the different absorption bands multiplied by appropriate weight factors. In this thesis, the reverse has been done to calculate the binding geometries of mononuclear ruthenium complexes: the experimentally obtained absorption and linear dichroism spectra have been divided into separate absorption bands, one for each polarization direction, by guessing values for the weight factors. The residual norm between the calculated and a set of reference absorption bands (see below) has then been minimized by varying the weight factors, with the minimum corresponding to the most probable binding geometry.

This analysis is only possible when the polarization and spectral shape of the absorption bands of the DNA binding ligand are known, and unfortunately, overlap of the absorption bands complicates also the determination of their polarizations and spectral shapes. However, for $[\text{Ru}(\text{phen})_2\text{dppz}]^{2+}$ the characteristics of the transition dipole moments have been fully assigned by Lincoln et al. using a combination of absorption, linear dichroism and emission anisotropy data.⁹¹⁻⁹³ The absorption bands obtained for $[\text{Ru}(\text{phen})_2\text{dppz}]^{2+}$ have been used in this thesis as references for determining the binding geometry of two new mononuclear ruthenium complexes with substituents in the 10- and 13-position of the dppz ligand, based on the assumption that the substituents do not significantly alter the spectral properties of the complexes.

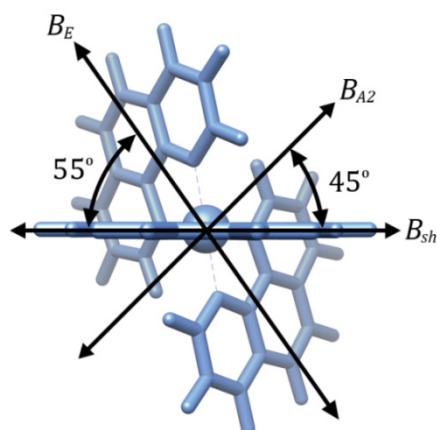


Figure 3.4. The orientation of the B polarized transition dipole moments depicted on the Δ -enantiomer of $[\text{Ru}(\text{phen})_2\text{dppz}]^{2+}$. The A polarized transition is oriented perpendicular to the plane of the paper along the long axis of the dppz ligand which is pointing out from the paper.

The absorption spectrum of $[\text{Ru}(\text{phen})_2\text{dppz}]^{2+}$ can be divided into four major absorption bands, each being polarized along one of the four major transition dipole moment directions A, B_E , B_{A2} , and B_{sh} (Figure 3.4). The A and B_{sh} polarized transitions, which are mainly associated with MLCT and $\pi \rightarrow \pi^*$ transitions localized on the dppz ligand, are polarized in the plane of the dppz ligand. In an intercalative binding geometry, these transitions will both be more or less perpendicular to the DNA helix, and are therefore treated as one transition dipole moment with $\alpha = 90^\circ$ in the analysis. The B_E and B_{A2} transitions originates mainly from MLCT and $\pi \rightarrow \pi^*$ transitions localized on the phenanthroline ligands and are polarized in a plane perpendicular to the long axis of the dppz ligand. The LD and LD^r of these transitions will, in an intercalative binding mode, be very sensitive to rotation around the dppz long axis. Thus, the binding mode of the new mononuclear ruthenium complexes have been determined by comparison of their calculated B_E and B_{A2} polarized absorption bands with those previously determined for $[\text{Ru}(\text{phen})_2\text{dppz}]^{2+}$ by the method described above.

Calculation of the angles α from the LD^r , and the method for determination of binding geometry described above, requires knowledge about the macroscopic orientation factor, which is denoted S in Equation 3.7. The orientation factor reflects how well the DNA molecules are aligned in the sample, and ranges from zero to one, where one corresponds to perfect orientation and zero to complete disorder. Here, the orientation factor has been estimated from the LD^r of pure DNA of equal concentration as in the ruthenium containing samples, assuming $\alpha = 90^\circ$ for the nucleobase absorption band at 260 nm. This is a simple method and gives a reasonable estimate of the orientation factor in the ligand containing samples, provided that binding of the ligand does not significantly alter the orientation of the DNA.

3.6 Studying DNA Binding by Circular Dichroism

In resemblance to the LD technique, circular dichroism (CD) spectroscopy is based on differences in absorbance of polarized light, but as the name implies circularly polarized light is used. In circularly polarized light the oscillation direction of the electric field rotates around the propagation direction, and the tip of the electric field vector traces out a helix in space. The helix can be either left handed or right handed, and CD is defined as the difference in absorbance between left and right handed circularly polarized light:

$$CD = A_l - A_r \quad \text{(Equation 3.8)}$$

Only chiral molecules and molecules perturbed by a chiral environment exhibit CD. Both DNA and the investigated ruthenium complexes are chiral, and thus exhibit CD signals on their own, but when studying DNA-ligand interactions the phenomenon of induced CD is much more useful. When small ligands, chiral or non-chiral, bind to the chiral DNA polymer in an orderly manner, their transition dipole moments will interact with the nucleobase transition dipole moments in such a way that they will exhibit a new CD signal, the induced CD, that is only present when the ligand interacts with DNA.⁸⁹ A change in the CD spectrum of a sample of DNA and ligand reflects a change in the interaction between the DNA and the ligand, and thus changes in binding geometry can be studied by CD. However, in contrast to LD, where there is a simple relation between the LD signal and the orientation of the chromophore, the origin of the induced CD signal is more complicated, especially when there are several different transition dipole moments involved. Consequently, it is difficult to directly relate the induced CD signal of the ruthenium complexes to a specific binding geometry, and therefore CD has been used in a more quantitative way in this thesis. It has previously been shown for the well studied threading intercalator $[\mu\text{-bidppzRu}_2(\text{phen})_4]^{4+}$ that threading results in a large positive induced CD signal in the visible region,^{75, 94} and similar spectral changes observed for the ruthenium complexes investigated in this thesis have been interpreted as rearrangement from an initial groove bound binding mode to threading intercalation.

3.7 Kinetic Characterization of Threading Intercalation

As mentioned in the introduction, one of the main characteristics of threading intercalation is the extremely slow association and dissociation kinetics compared with other DNA binding modes. Therefore, in absence of structural information such as NMR or crystallography data, kinetic studies have become the main technique to confirm that a compound binds DNA by threading intercalation.³³ The threading intercalation kinetics has been thoroughly studied for the parent compound $[\mu\text{-bidppz}(\text{phen})_4\text{Ru}_2]^{4+}$, and much of the current knowledge regarding the kinetic behavior of this complex is relevant also for the complexes studied here considering their similar structure and DNA binding modes.

It was early discovered that the ruthenium complex rapidly binds to the groove of the DNA, after which the much slower rearrangement to the threaded state takes place.⁷³ Thus, the threading event can, at least at low binding ratios, be seen as a unimolecular reaction occurring from the groove bound state, where there is a pre-equilibrium between complexes in the groove bound state and free in solution (Figure 3.5). The observed reaction rate for the threading event can therefore be described by Equation 3.9 where the first term on the right hand side describes the threading event from the groove bound state. The second term accounts for dissociation of complexes from the threaded state, which also has to be included in the model since there is an equilibrium also between the threaded state and the other states.⁷⁴⁻⁷⁵

$$\frac{d[C]}{dt} = k_2 \frac{k_1}{k_{-1}} [B] - k_{-2} [C] \quad (\text{Equation 3.9})$$

Provided that the threading association rate constant is much larger than the corresponding dissociation rate constant and that the equilibrium between groove bound and free complex is shifted towards the groove bound form, it is evident from Equation 3.9 that the kinetic trace for mixing complex with DNA should be mono-exponential with a rate constant corresponding to the threading intercalation rate constant. This is indeed the case when the threading reaction is monitored by CD, but when studied by emission spectroscopy the kinetic traces are multi-exponential. Detailed studies of this phenomenon have shown that the fastest exponential of the emission traces corresponds to the threading event, and the other exponentials have been assigned to redistribution of threaded complexes along the DNA polymer.⁷⁵ When the dissociation rate constant is larger than or of the same magnitude as the association rate constant, studies of the association kinetics is complicated by the fact that also the dissociation rate contributes to the observed kinetic trace, and the association rate constant cannot be accurately determined.

A well established method to study dissociation kinetics of hydrophobic and cationic molecules from DNA is to induce dissociation by addition of a detergent such as sodium dodecyl sulfate (SDS) to equilibrated samples of ligand and DNA.⁹⁵ The detergent will, provided that the concentration is high enough, form micelles that act as a sequestering agent that captures ligands that are free in solution, thus shifting the equilibrium towards unbound ligand. Since there is no ligand free in solution no binding reaction occurs, and the dissociation rate constant can be determined by monitoring how the amount of bound complex changes with time. However, SDS has been shown to catalyze the dissociation of ruthenium complexes as well as other ligands from DNA^{7, 76, 96} and therefore the dissociation rate constants determined by this method, as the ones reported here, should be interpreted with caution.

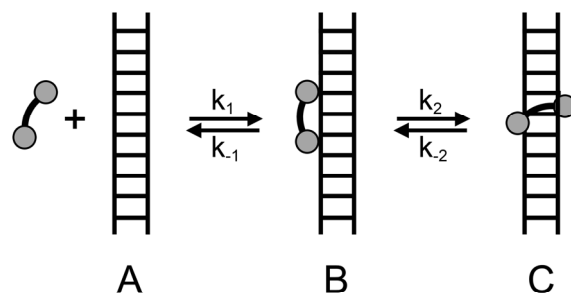


Figure 3.5. Schematic picture of the threading event. The complex rapidly binds externally on the DNA, from where threading occurs.

The criterion that the kinetics of a threading intercalating compound should be significantly slower than for its non-threading analogues is somewhat ambiguous, and the rate constants for both threading and non-threading interactions vary greatly between different classes of compounds.^{7, 33, 44-45, 49, 56, 73} Therefore, it is not possible to determine a general cutoff value for the rate constant that distinguishes threading intercalation from other binding modes, but instead the measured rate constants have to be compared with those of known threading intercalators and non-threading compounds of the same class. The rate constants for SDS induced dissociation from ct-DNA for the mononuclear non-threading complex $[\text{Ru}(\text{phen})_2\text{dppz}]^{2+}$ and the known threading intercalator $[\mu\text{-bidppz}(\text{phen})_4\text{Ru}_2]^{4+}$, which at room temperature are in the order of $1\text{-}10\text{ s}^{-1}$ and $10^{-3}\text{-}10^{-4}\text{ s}^{-1}$ respectively, can be used as reference values for the numbers reported in this thesis.^{73, 97} The kinetics has mainly been studied by monitoring the change in emission or the induced CD signal in the visible region with time, but also absorbance spectroscopy has been used to study the mononuclear disubstituted dppz complexes which are non-luminescent.

3.8 Binding Thermodynamics and Isothermal Titration Calorimetry

While there are a number of available methods to determine the equilibrium constant K , and hence the free energy change ΔG of a binding event, the binding enthalpy ΔH can be directly assessed only by calorimetric methods. In isothermal titration calorimetry (ITC) the ligand is titrated into the sample cell containing the macromolecule (or vice versa). The heat evolved or absorbed upon each addition of ligand is measured as the heat flow required to or from the sample cell to maintain the cell at the same temperature as a reference cell of equal volume. The enthalpy change for each injection is obtained as the integrated heat flow, from which the binding enthalpy can be determined provided that the concentrations of ligand and macromolecule are known.

In the simplest system, where the binding sites on the macromolecule are independent and ligand binding is non-cooperative, the ITC curve will have a

sigmoidal shape. For the first few injections, virtually all injected ligand binds the macromolecule since there are many free binding sites available, and the integrated heat reflects the binding enthalpy. As the binding sites gradually become saturated, only a fraction of the injected ligand will bind the macromolecule and the observed enthalpy change will decrease resulting in a curved region in the ITC profile, where the curvature depends on K and the total number of binding sites. Eventually, when all binding sites are occupied by ligands, further addition of ligand will not result in any binding. The enthalpy change for these last few injections would, since no binding occurs, ideally be due only to dilution of ligand, which can be measured and corrected for by a separate experiment where ligand solution is titrated into buffer. However, also differences in the buffer composition, such as differences in ion concentration or pH, may result in an additional heat of mixing. To minimize these effects, the macromolecule solution is dialyzed against a large volume of buffer, and the ligand solution is then prepared by diluting the ligand in the dialysate.⁹⁸

As mentioned above, the integrated heat of the first few injections reflects the binding enthalpy, but since the amount of bound ligand for each injection in reality depends on K also at low ligand concentrations iterative fitting of a theoretical binding isotherm to the data has to be employed to determine ΔH accurately. The integrated heat for each injection Q_i is related to the binding enthalpy ΔH according to Equation 3.10, where the molar increase of bound ligand with each injection is given by $\Delta[L_i]_{bound} \times V_{cell}$.

$$Q_i = \Delta[L_i]_{bound} V_{cell} \Delta H \quad (\text{Equation 3.10})$$

In the regression procedure, $\Delta[L_i]_{bound}$ is calculated for each injection based on the known total concentration of added ligand and guessed values for K and the total concentration of binding sites. The best values for ΔH , K and the number of binding sites on each macromolecule are obtained by minimizing the error between the calculated and experimental values for Q_i .⁹⁸⁻⁹⁹ Once ΔH and K has been determined, ΔG and ΔS for the binding reaction can be obtained from the following relations:

$$\Delta G = -RT \ln K \quad (\text{Equation 3.11})$$

$$\Delta G = \Delta H - T \Delta S \quad (\text{Equation 3.12})$$

By calorimetric studies at several different temperatures, the heat capacity change for the reaction ΔC_p can be obtained from the slope of a plot of ΔH versus T . ΔC_p is defined as the difference in heat capacity between products and reactants, and describes how ΔH and ΔS varies with temperature. As there is a correlation between ΔC_p and changes in surface area accessible to solvent, the magnitude of ΔC_p reflects the contribution of hydrophobic interactions to the binding free energy.⁹⁹⁻¹⁰²

3.9 Binding Isotherms and the McGhee-von Hippel Model

When the binding sites on the macromolecules are independent and isolated, which is often the case for proteins and short oligonucleotides with one defined binding site, the above analysis is relatively straight forward. However, the DNA used in the experiments presented here, poly[dAdT]₂, are long polymers of binding sites, which overlap each other if the ligand occupies more than one base pair when bound. Furthermore, if the bound ligands interact with each other, the interactions may be either cooperative or anti-cooperative and give rise to an interaction enthalpy Δh in addition to the intrinsic binding enthalpy ΔH . In 1974 McGhee and von Hippel presented a method for calculation of the fraction of bound ligands that accounts for both ligand-ligand interactions and ligands covering more than one base pair.¹⁰³ If a ligand binds DNA with two different binding geometries the McGhee-von Hippel theory for two distinct ligands competing for the same binding sites on the DNA can be used to calculate the binding isotherms. The mass balance equations for the two bound species are coupled though, because there is no difference between the ligands when free in solution and both bound species consequently are in equilibrium with a common pool of free ligands. However, if the cooperativity parameters are not unity, as for the ruthenium complexes investigated in Paper IV, the original McGhee-von Hippel equations of can no longer be used. Instead, a matrix-based generalized McGhee-von Hippel method is required, which is briefly summarized below.¹⁰⁴

In the McGhee-von Hippel theory the DNA is treated as a one dimensional lattice of binding sites (residues), and conditional probabilities are used to calculate the number of free binding sites and occurrence of ligand-ligand interactions. The probability of finding a ligand of type i bound to a randomly chosen binding site is given by the binding density θ_i , which is defined as the ratio between the concentration of bound ligand i and the total concentration of binding sites. The probability that a residue occupied by a ligand of type i is followed a residue occupied by a ligand of type j when moving in one direction along the lattice, is denoted p_{ij} , and the cooperativity parameter for the interaction is denoted y_{ij} . The conditional probabilities p_{ij} for all possible combinations of a ligand binding next to another ligand or a free base pair are assembled into the matrix \mathbf{P} . Similarly, the elements of the matrix \mathbf{Y} gives the cooperativity parameters for the corresponding interactions. The propability of finding a free base pair (which is defined as type 1) on the DNA lattice is given by $\theta_1 = 1 - \sum n_i \theta_i$ where n_i is the number of base pairs made inaccessible by the bound ligand and the summation is over all types of bound ligands. The vector $\mathbf{e} = [1 \dots 1]$ and the transposition of the vector $\boldsymbol{\theta} = [\theta_1 \dots \theta_N]$ containing the binding densities for all types of bound species i , are right and left hand eigenvectors to \mathbf{P} , respectively and are used to rearrange Equation 3.13 into Equation 3.14 and 3.15 (see below).

To calculate the binding and interaction enthalpies and simulate ITC data, the amount of ligand bound and ligand-ligand interactions in each titration step has to be found. Thus, the objective of the McGhee-von Hippel analysis is, given binding

constants K_i , cooperativity parameters y_{ij} , and binding site sizes n_i , to find a θ that satisfy the mass balance equations, i.e. the total amount of ligand in the calculations L_{calc} should equal the total amount of ligand added during the experiment L_{added} , which in addition to the total concentration of binding sites $[B]_{tot}$ is known. This is done by guessing values for K_i , y_{ij} , n_i , and θ , which are then optimized by iteration as follows: The cooperativity parameters can be converted into conditional probabilities by multiplication with the matrices \mathbf{S} and \mathbf{R} (Equation 3.13), which are diagonal matrices with positive elements such that $p_{ij} = s_i y_{ij} r_j$. \mathbf{S} and \mathbf{R} are found by iteration using Equations 3.13 and 3.14 until $\mathbf{r}_{k+1} = \mathbf{r}_k$, where \mathbf{r} and \mathbf{s} are column vectors containing the diagonal elements of \mathbf{R} and \mathbf{S} , respectively.

$$\mathbf{P} = \mathbf{S}\mathbf{Y}\mathbf{R} \quad (\text{Equation 3.13})$$

$$\mathbf{s}_k = 1./(\mathbf{Y}\mathbf{r}_k) \quad (\text{Equation 3.14})$$

$$\mathbf{r}_{k+1} = \theta./(\mathbf{Y}^T \mathbf{S}_k \theta) \quad (\text{Equation 3.15})$$

The binding potential x_i and the free ligand concentration $[L]$ is calculated by inserting the elements of \mathbf{S} and \mathbf{R} into Equation 3.16, which in turn are used to calculate L_{calc} according to Equation 3.17. The error between L_{calc} and L_{added} is then minimized by a Newton-Raphson algorithm where θ is varied.

$$x_i = K_i [L] = \frac{[L_i B]}{[B]} = \frac{p(L_i B)}{p(B)} = \frac{p_{1i} p_{i1}}{p_{11}^{n_i+1}} = \frac{s_i r_i}{p_{11}^{n_i}} \quad (\text{Equation 3.16})$$

$$L_{calc} = [L]_{free} + [L]_{bound} = \frac{x_i}{K_i} + [B]_{tot} \sum \theta_i \quad (\text{Equation 3.17})$$

The concentrations of the bound ligands L_i in each titration step is obtained from the optimized θ , as are the concentrations of the different combinations of interactions using Equation 3.18. Thus, the change in the concentrations for each titration step can be obtained and ΔH and Δh calculated from a least square fit to the experimental data. The error between the fitted and experimental heat per injection is then minimized by varying K_i , y_{ij} , and n_i .

$$\theta_{ij} = \theta_i p_{ij} \quad (\text{Equation 3.18})$$

3.10 Studying Cell Interactions by Confocal Microscopy

DNA binding studies in simple and well-defined systems are important to obtain detailed mechanistic knowledge of the binding event. In living cells, however, the DNA is found in a much more complex environment consisting of lipid structures, proteins, RNA, ions and small organic molecules, which may interfere with DNA binding. Therefore, it is of great importance to also study how the complexes

interacts with cells, which is done in Paper V. This section gives a short description of the cellular structures discussed in the results section and how the interactions between ruthenium complexes and such structures were studied.

All cells are surrounded by a phospholipid bilayer, the plasma membrane, which in addition to defining the boundaries of the cell also serves as a protective barrier by only allowing certain specific molecules to enter or leave the cell. Inside eukaryotic (e.g. mammalian) cells, a number of membrane enclosed compartments are found, such as mitochondria, the Golgi apparatus and the endoplasmic reticulum, which are commonly referred to as organelles. All organelles have specific functions, and the most important organelle for this work is the nucleus, in which the DNA is lodged and replication as well as transcription occurs. The nucleus also contains well-defined but non-membrane enclosed structures termed nucleoli, where ribosomal RNA is synthesized. The contents inside the plasma membrane, excluding the organelles, is termed the cytosol, which is where the messenger RNA produced in the nucleus is translated into proteins. Thus, the cytosol contains both RNA and proteins, as well as a wide variety of other biomolecules. To exert its action, a DNA targeted drug has to pass the plasma membrane and diffuse through the cytosol without being trapped by interactions with other molecules to finally enter the nucleus where it can bind the DNA. Highly charged molecules, as the ones studied here, are unlikely to pass the plasma membrane by diffusion due to the hydrophobic interior of the lipid bilayer. There are other possible uptake mechanisms though, such as endocytosis, where extracellular fluid is captured inside lipid vesicles, endosomes, by the formation of invaginations in the plasma membrane that bud off into the cytosol. If the drug is internalized by this mechanism it may be eventually be released into the cytosol if the endosome ruptures, provided that it has not been degraded by then.¹²

An excellent technique to visualize the localization of emissive molecules inside cells, and thus their preferences for various biomolecules, is fluorescence confocal laser scanning microscopy (CLSM). In short, the chromophores are excited by a focused laser beam and only emission from the focal point is detected. By moving the focal point across a plane in the sample, two-dimensional images with high spatial resolution can be created (see for example the textbook of Pawley for technical details¹⁰⁵). The localization of the imidazophenanthroline complexes is readily studied by CLSM since they are highly emissive and their quantum yields rather insensitive to the environment, but the threading intercalating light-switch complexes are only detectable when bound to hydrophobic structures. In this work, the interactions with both live and fixed cells, where the plasma membrane has been permeabilized by addition of cold methanol to the cells, are studied. The advantage of fixation is that the preferences for various biomolecules can be investigated in the intracellular milieu, since the uptake is not limited by poor transport over the plasma membrane, whereas live cell studies reflects what would actually happen to the complexes inside cells.

4 RESULTS

The aim of this work is to investigate the relationship between ruthenium complex structure and selective DNA binding. The study is primarily focused on binuclear ruthenium complexes with phenanthroline auxiliary ligands, where the effect of bridging ligand structure and chirality around the ruthenium centers on AT-selective DNA threading intercalation is investigated (Paper I-II). Also, a new type of mononuclear threading intercalating complexes, with a substitution pattern on the intercalating ligand that is different from all previously published threading complexes, has been developed (Paper III). Further, the DNA binding of the non-threading mononuclear complexes $[\text{Ru}(\text{phen})_2\text{dppz}]^{2+}$ and $[\text{Ru}(\text{bpy})_2\text{dppz}]^{2+}$, which correspond to the smallest common structural part of all known threading intercalating ruthenium complexes, has been investigated with isothermal titration calorimetry to better understand the nature of the interactions between the complexes and DNA (Paper IV). Finally, cell studies on several binuclear complexes have been performed to investigate how the results from the DNA binding studies in simple systems, such as pure DNA, correlates with the DNA binding properties in the more complex milieu inside cells (Paper V). This chapter summarizes the main results of Paper I-V and also presents some relevant unpublished data.

4.1 Bridging Ligand Structure

Despite numerous DNA binding studies on binuclear polypyridyl ruthenium complexes of similar size and shape as the known threading intercalator $[\mu\text{-bidppz}(\text{phen})_4\text{Ru}_2]^{4+}$, there are few reports of threading intercalating complexes.¹⁰⁶⁻¹¹⁶ In addition to the thoroughly studied bidppz complexes, with 1,10-phenanthroline, 2,2'-bipyridine or [12]aneS₄ as auxiliary ligands,^{73, 75} the only binuclear ruthenium complexes known to bind DNA by threading intercalation are their rigid analogue $[\mu\text{-dtpf}(\text{phen})_4\text{Ru}_2]^{4+}$ and the flexible bis-intercalator $[\mu\text{-C4}(\text{cpdppz})_2(\text{phen})_4\text{Ru}_2]^{4+}$.^{35-36, 117} Common to these complexes is that they all contain dppz-moieties, and therefore we wanted to investigate whether this structure is necessary for threading intercalation to occur. In Paper I we compare threading ability of three binuclear complexes with systematically varied bridging ligands: the parent complex $[\mu\text{-bidppz}(\text{phen})_4\text{Ru}_2]^{4+}$ (**1**) with two dppz-moieties, and $[\mu\text{-}m\text{-bipb}(\text{phen})_4\text{Ru}_2]^{4+}$ (**2**) and $[\mu\text{-dppzip}(\text{phen})_4\text{Ru}_2]^{4+}$ (**3**), with no and one dppz-moieties, respectively (Figure 4.1).

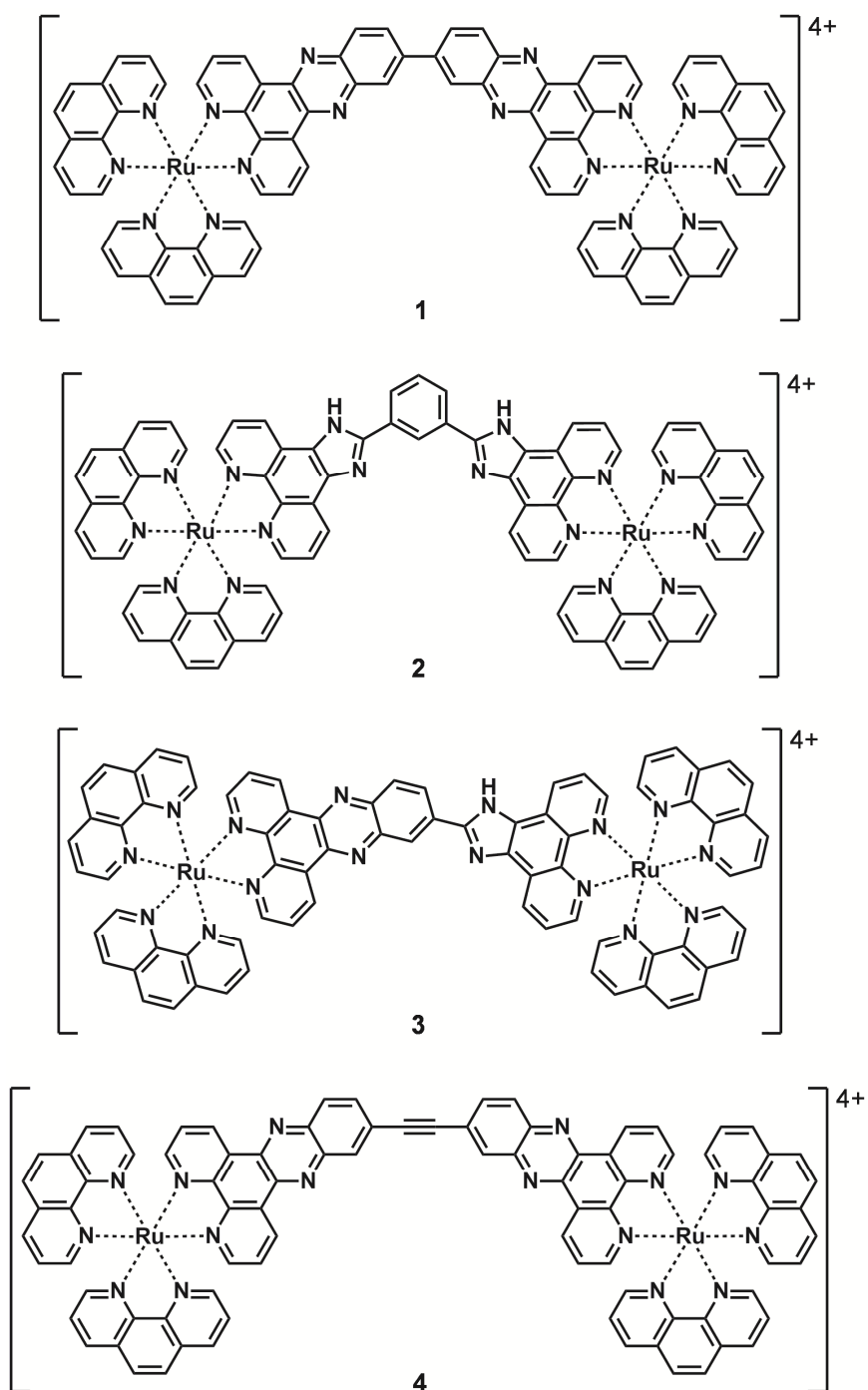


Figure 4.1. Structures of the investigated binuclear complexes: $[\mu\text{-bidppz}(\text{phen})_4\text{Ru}_2]^{4+}$ (**1**), $[\mu\text{-}m\text{-bipb}(\text{phen})_4\text{Ru}_2]^{4+}$ (**2**), $[\mu\text{-dppzip}(\text{phen})_4\text{Ru}_2]^{4+}$ (**3**), and $[\mu\text{-bidppze}(\text{phen})_4\text{Ru}_2]^{4+}$ (**4**).

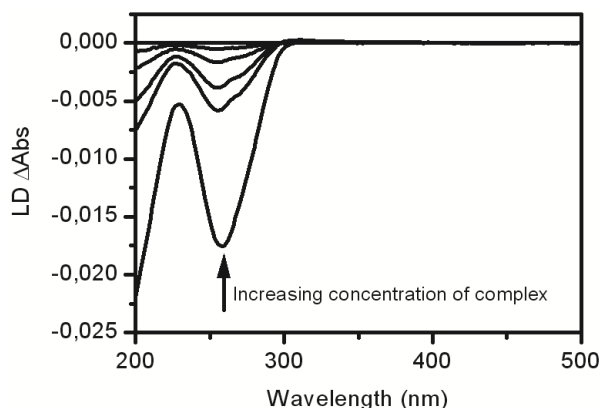


Figure 4.2. LD spectra of ct-DNA ($\sim 100 \mu\text{M}$) in presence of increasing concentrations of $\Delta\Delta\text{-2}$ ($[\text{Ru}]/[\text{bp}] = 0, 1/18, 1/16, 1/12, 1/11, 1/10$) at 150 mM NaCl . The decreasing amplitude of the DNA-signal at 260 nm indicates compaction of the DNA as the complex concentration increases.

Complex **2** has essentially the same shape as **1**, but is expected to be more flexible compared with the other two complexes since the bridging ligand has two instead of one single bond where rotation can occur. Since threading intercalation of **1** has been proposed to locally distort the B-conformation of the DNA to a more A-form like structure⁷⁸ increased flexibility was believed to improve threading ability. If the complex could adapt its conformation to fit the DNA better, this would reduce the stress on the DNA and the B-conformation could be maintained. Contrary to what we expected, **2** does not appear to thread DNA at all. LD experiments show loss of the DNA orientation with increasing concentration of **2**, as seen by the decrease of the DNA-signal amplitude in Figure 4.2, indicating compaction of the DNA. In Paper V, the DNA binding properties of an isomer of **2** with *para*-substitution on the bridging ligand benzene ring was investigated. This complex also compacts ct-DNA and exhibits no signs of threading intercalation.

Complex **3**, on the other hand, binds AT- but not ct-DNA by threading intercalation. This is seen by the slow increase in luminescence intensity with time upon addition of AT-DNA to the complex and the absence of such intensity changes in presence of ct-DNA (Figure 4.3). The dissociation rate constants for both enantiomers are approximately 1-2 orders of magnitude larger than for **1**, but still much smaller than for non-threading compounds, confirming that the binding mode with AT-DNA is indeed threading intercalation. The faster dissociation, combined with the fact that the threading process is slower, indicates that the threading intercalation binding constant is significantly smaller for **3** compared with **1**. Complex **3** appears to be just at the border of being capable of threading intercalation as judged from photophysical experiments (see section 4.2). While $\Delta\Delta\text{-3}$ readily threads AT-DNA, only a small fraction of $\Delta\Delta\text{-3}$ is threaded at

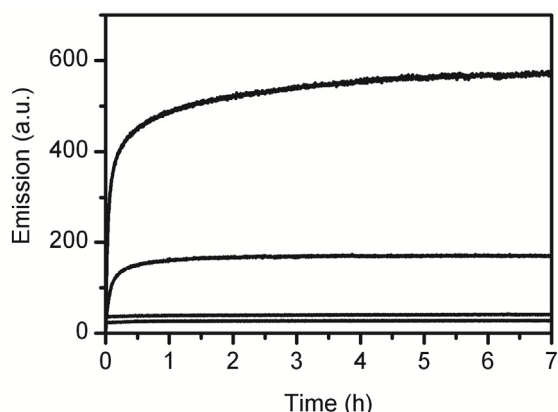


Figure 4.3. Association kinetics of complex **3** at 50 °C and 150mM NaCl. From top to bottom: $\Lambda\Lambda$ -**3** + AT-DNA, $\Delta\Delta$ -**3** + AT-DNA, $\Delta\Delta$ -**3** + ct-DNA and $\Lambda\Lambda$ -**3** + ct-DNA. The slow increase in luminescence in presence of AT-DNA indicates that the binding mode is threading intercalation.

equilibrium. This was later confirmed also by CD and LD experiments as well as kinetic studies in Paper II. The reduced binding constant for **3** is proposed to be an effect of the bridging ligand being slightly shorter than for **1**, causing the phenanthrolines on both ruthenium centers to be in close contact with the DNA in the threaded state, thus increasing the stress exerted on the DNA by the threaded complex. This would be expected to result in the interaction being more sensitive to the flexibility of the DNA, which can explain the greater AT-selectivity of **3** compared with the parent complex **1**.

To further investigate this hypothesis, a binuclear complex with an elongated bridging ligand, $[\mu\text{-bidppze}(\text{phen})_4\text{Ru}_2]^{4+}$ (**4**), was synthesized and examined (Figure 4.1). Both enantiomers of **4** seem to initially compact the ct-DNA as seen by the absence of complex signals and a reduced amplitude of the DNA-signal in LD spectra recorded immediately after mixing. However, pronounced complex signals with the same characteristics as the ones for threaded **1** emerge for the $\Delta\Delta$ -enantiomer after 20 h incubation at 50 °C, indicating that $\Delta\Delta$ -**4** bind DNA by threading intercalation (Figure 4.4). For the $\Lambda\Lambda$ -enantiomer the complex signals were barely visible even after prolonged incubation, suggesting that the majority of the complexes remain externally bound also at equilibrium. Comparison of the association rates for ct- and AT-DNA shows that the AT-selectivity is more or less lost when the bridging ligand length increases supporting the above hypothesis (Figure 4.4). Whether the threading intercalation binding constant is larger for **4** than **1** remains to be investigated.

Although the bridging ligand length clearly affects the threading intercalation properties of binuclear ruthenium complexes, conservation of the bridging ligand length alone is not sufficient to maintain threading intercalation ability. Instead, the presence of a dppz-moiety seems more important for this type of

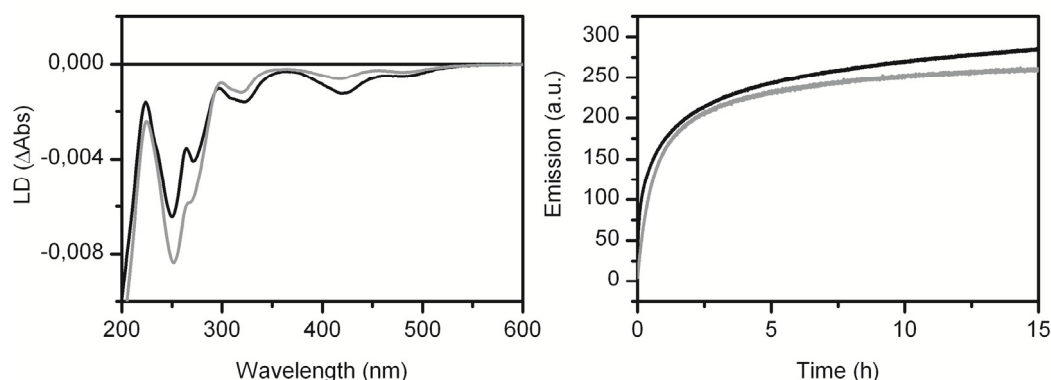


Figure 4.4. Left: LD spectra of $\Delta\Delta$ -4 (black) and $\Delta\Delta$ -1 (grey) bound to ct-DNA after 20 h incubation at 50 °C. Right: Kinetic traces for the association of $\Delta\Delta$ -4 to AT- (black) and ct-DNA (grey) at 50 °C. Both experiments were performed at 50 mM NaCl.

binding, as seen by the fact that **3** and $\Delta\Delta$ -4 which contain dppz-moieties thread DNA while the two isomers of **2** do not. This can be due to the fact that the imidazophenanthroline(ip)-moiety has a smaller hydrophobic surface than the dppz-moiety, making intercalation of the bridging ligand of **2** less favorable. It is also possible that the **2**-isomers interact much more favorably with the DNA when bound in the groove as a result of the increased flexibility and hydrogen bonding capacity. Recently, an analogue to the *para*-substituted **2**, with an elongated bridging ligand, has been synthesized and assayed for threading intercalation but neither this complex threads DNA, consistent with the above results.¹¹⁸

4.2 Enantioselectivity and Enantiomeric Preferences of the Grooves

As described above, threading intercalation of **3** is more efficient for the $\Lambda\Lambda$ - than the $\Delta\Delta$ -enantiomer, which is contrary to what is observed for threading of **1** into AT-DNA.⁷⁵ To investigate the origin of this reversed enantioselectivity, the DNA binding of the “*meso*” enantiomeric pair of **3** (denoted $\Delta\Lambda$ and $\Lambda\Delta$, where the first and second symbol refer to the chirality on the dppz- and ip-part, respectively) was studied in Paper II. Since **3** is asymmetrical, it is possible to distinguish which part of the bridging ligand that is stacked between the DNA base pairs, and thus how the chirality on the intercalated and non-intercalated halves affects binding, respectively. Based on the observation of a light-switch effect upon threading and the fact that the dppz-moiety seems important for threading to occur, it was concluded that the dppz-part of the bridging ligand is stacked between the base pairs.

From photophysical data for the four isomers of **3** in presence of AT-DNA (Table 4.1) it is evident that $\Delta\Lambda$ has the largest threading intercalation binding constant, followed by $\Lambda\Lambda$, $\Delta\Delta$, and finally $\Lambda\Delta$. Kinetic studies reveal the same

Table 4.1. Photophysical data for the four isomers of **3** bound to AT-DNA.

Sample ^a	$\tau_1 / \text{ns} (\alpha_1)$	$\tau_2 / \text{ns} (\alpha_2)$	$\tau_{\text{avg}}^b / \text{ns}$	Φ^c	$\tau_{\text{rel}}^d / \text{ns}$	% bound ^e
$\Delta\Delta$	51 (0.80)	559 (0.20)	153	0.15	1021	17
$\Delta\Lambda$	54 (0.43)	270 (0.57)	177	1	177	100
$\Lambda\Delta$	51 (0.77)	559 (0.23)	168	0.11	1550	11
$\Lambda\Lambda$	54 (0.47)	270 (0.53)	168	0.83	202	88

^a120 μM nucleotides and 3.75 μM complex in 150 mM NaCl at 25 °C. ^bAverage emission lifetime calculated as $\tau_{\text{avg}} = \alpha_1\tau_1 + \alpha_2\tau_2$. ^cRelative quantum yields calculated by normalization of the integrated emission spectra against the integrated spectrum for $\Delta\Lambda$. ^dRelative intrinsic lifetimes calculated from $\tau_{\text{rel}} = \tau_{\text{avg}}/\Phi$. ^ePercentage of bound complex calculated as the ratio between τ_{rel} for $\Delta\Lambda$ and τ_{rel} for the complex based on the assumptions that all $\Delta\Lambda$ is bound and that the intrinsic lifetime is the same for all isomers.

pattern, with $\Delta\Lambda$ displaying the largest and $\Lambda\Delta$ the smallest ratio between the association and dissociation rate constants. The differences in association rates are modest, and the different binding constants appear to mainly be caused by variations in the dissociation rate (Figure 4.5). Moreover, the shape of the LD and CD spectra in presence of AT-DNA changes dramatically with time for $\Delta\Lambda$ and $\Lambda\Delta$, while the spectra for $\Delta\Delta$ and $\Lambda\Lambda$ remain essentially the same (Figure 4.6). This reflects a rearrangement from an initial groove bound state to an intercalated geometry for the main part of the $\Delta\Lambda$ - and $\Lambda\Delta$ -complexes, but suggests that the spectra for $\Delta\Delta$ and $\Lambda\Delta$ are dominated by the groove bound form also at equilibrium. All together, these results show that Δ is the optimal configuration on the ruthenium center of the intercalating dppz-part while Λ -geometry is more favorable on the non-intercalating ip-part.

The LD and LD^r spectra immediately after mixing with AT-DNA are very similar for all four isomers, indicating similar initial binding modes. Also, the LD^r spectra in presence of ct-DNA, where threading does not occur, are nearly identical to those immediately after mixing with AT-DNA (Figure 4.7). This indicates that the initial binding is similar for the two types of DNA and that the difference in threading ability lies in the threaded state rather than in the initial groove bound state. $\Delta\Lambda$ appears to have the best structure to fit the threading intercalation binding site, and the larger flexibility of AT-DNA allows better accommodation of the threaded complex than the more rigid ct-DNA. Kinetic studies further support these conclusions since there are larger differences between the isomers in the SDS induced dissociation rates than in the association rates.

Comparison of the threading properties of $\Lambda\Lambda$ and $\Delta\Delta$, which both have one ruthenium center with “correct” chirality, shows that the geometry around the ruthenium on the ip-part has a stronger influence on the threading ability than the geometry of the dppz-ruthenium center. This is somewhat surprising considering the fact that the dppz-moiety is assumed to intercalate the DNA, but provides an

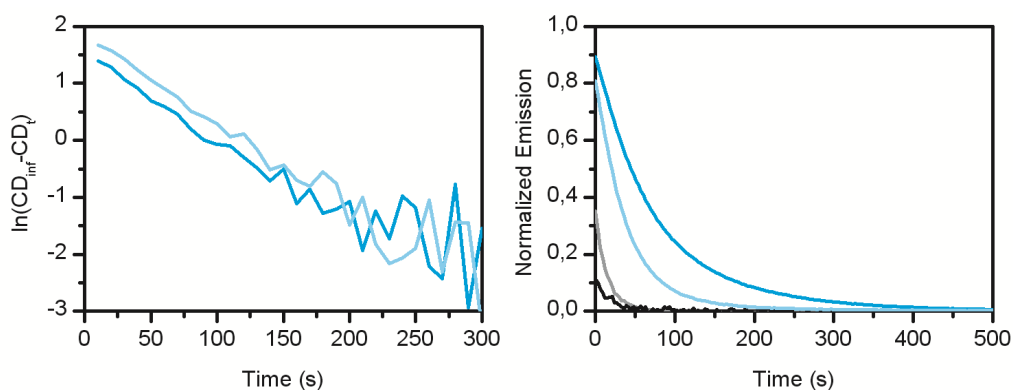


Figure 4.5. Left: association kinetics of $\Delta\Lambda$ -**3** (dark blue) and $\Lambda\Lambda$ -**3** (light blue) to AT-DNA studied by CD spectroscopy at 50 °C. Both complexes display first order kinetics with similar rate constants. Right: dissociation kinetics of $\Delta\Lambda$ -**3** (dark blue), $\Lambda\Lambda$ -**3** (light blue), $\Delta\Delta$ -**3** (grey) and $\Lambda\Lambda$ -**3** (black) from AT-DNA studied by fluorescence spectroscopy at 50 °C. Dissociation was induced by addition of a stock solution of 3 % SDS to equilibrated samples of complex (3.5 μ M) and DNA (120 μ M) to a final concentration of 0.6 % SDS. The kinetic traces have been corrected for dilution and normalized against the emission intensity before addition of SDS. The kinetic traces are bi-exponential and the four isomers exhibit significant differences in dissociation rate constants.

explanation for the reversed enantioselectivity with respect to **1** and **4**. For complexes with short bridging ligands, also the phenanthrolines of the ruthenium center on the non-intercalating half are supposedly in close contact with the DNA, and are, as in the case of **3**, dominating the stereoselectivity. However, as the bridging ligand becomes longer, as when going from complex **3** to **1**, the stress exerted on the DNA by the phenanthrolines of the non-intercalating half will not be as large and the importance of these interactions will decrease. Instead, the geometry around the ruthenium of the intercalating part will be dominating. Since the intercalating parts of **1** and **4** are more or less identical to that of **3**, it is likely that Δ -geometry is the optimal configuration on the ruthenium on the intercalating half also for these complexes, resulting in the reversed enantioselectivity. The fact that the $\Lambda\Lambda$ -enantiomer of **4** does not seem to thread DNA at all while the same enantiomer of **1** does, suggest that the non-intercalating part of **1** also interacts with the DNA in the threaded state, enabling threading intercalation of $\Lambda\Lambda$ -**1** despite the fact that Δ is the optimal configuration on the intercalating part. For **4**, the phenanthrolines of the non-intercalating part do not seem to be able to make favorable interactions with the DNA, at least not in the Λ -configuration, and hence do not compensate for the less favorable interactions of the Λ -geometry on the intercalating half. The fact that the long emission lifetime of **3** is controlled by the chirality on the non-intercalating half shows that the phenanthrolines on this part of the complex are in close contact with the DNA in the threaded state and has great influence on the binding geometry, which supports the above explanation.

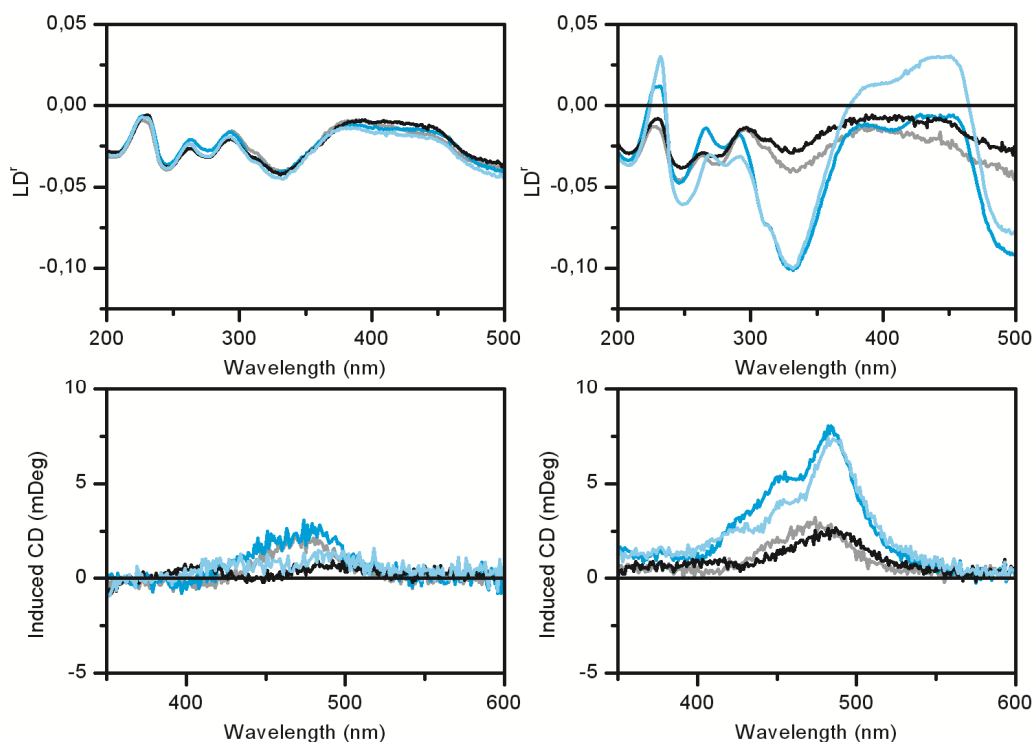


Figure 4.6. LD_r spectra (top) and induced CD (bottom) of $\Delta\Delta$ -3 (dark blue), $\Lambda\Lambda$ -3 (light blue), $\Delta\Lambda$ -3 (grey) and $\Lambda\Delta$ -3 (black) in presence of AT-DNA immediately after mixing (left) and at equilibrium (right). $\Delta\Delta$ -3 and $\Lambda\Lambda$ -3 display dramatic spectral changes with time indicative of threading intercalation, whereas only minor changes are observed for $\Delta\Lambda$ -3 and $\Lambda\Delta$ -3. The LD_r spectra of $\Delta\Lambda$ -3 and $\Lambda\Delta$ -3 at equilibrium have been multiplied by a factor 2 for ease of comparison since these samples have lower orientation as judged from the DNA-signal. The experiments were performed at 150 mM NaCl with 3.5 μ M complex and 120 μ M DNA.

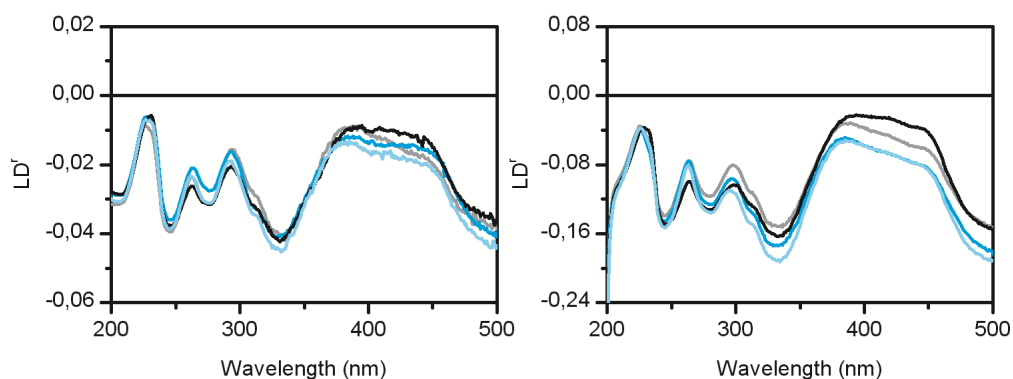


Figure 4.7. LD_r spectra of $\Delta\Delta$ -3 (dark blue), $\Lambda\Lambda$ -3 (light blue), $\Delta\Lambda$ -3 (grey) and $\Lambda\Delta$ -3 (black) in presence of AT-DNA (left) and ct-DNA (right) immediately after mixing. The similar spectral shapes indicate similar binding modes for all four isomers with both types of DNA.

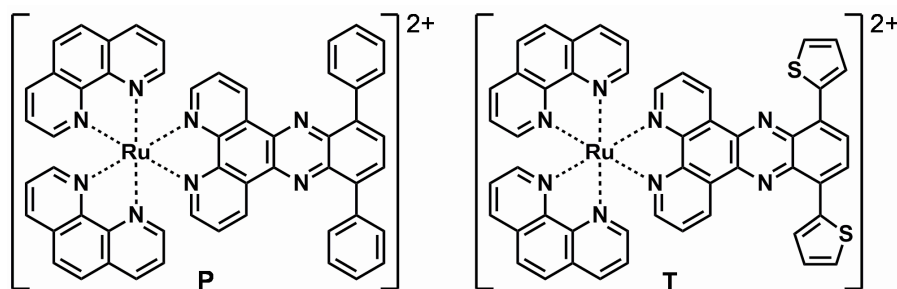


Figure 4.8. Structures of the two new ruthenium complexes $[Ru(phen)_2(10,13\text{-diphenyl}\text{-}dppz)]^{2+}$ (**P**) and $[Ru(phen)_2(10,13\text{-di}(2'\text{-thienyl})dppz)]^{2+}$ (**T**).

4.3 A New Substitution Pattern for Threading Intercalating dppz Complexes

Aside from the rigid complex $[\mu\text{-dtpf}(phen)_4Ru_2]^{4+}$ and the bis-intercalator $[\mu\text{-C4}\text{-}(cpdppz)_2(phen)_4Ru_2]^{4+}$, all ruthenium complexes, both mono- and binuclear, reported to bind DNA by threading intercalation contains a dppz-moiety with a positively charged bulky substituent in the 11-position.^{73, 75, 119-120} In Paper III, we have explored a new substitution pattern for threading intercalating mononuclear ruthenium complexes, where phenyl (**P**) or thienyl (**T**) substituents have been attached to the dppz ligand in 10- and 13-position (Figure 4.8). This substitution pattern provides a new strategy for development of mononuclear threading intercalating complexes, but the binding is very sensitive to the nature of the aryl substituents.

Figure 4.9 shows a comparison of the LD^r spectra of the DNA-bound enantiomers of **P** and **T** with the corresponding spectra of $[Ru(phen)_2dppz]^{2+}$, which is known to bind DNA by intercalation of the dppz ligand. The similarities of the LD^r spectra suggest that also **P** and **T** intercalate DNA by insertion of the aryl-substituted dppz ligand between the base pairs. Calculations of the roll angles for **P** and **T** from LD^r data, i.e. how the short axis of the dppz ligand is oriented relative to the DNA helix axis, resulted in values that are consistent with intercalation of the dppz ligand for both complexes (Table 4.2).

Despite these indications of similar binding modes for **P** and **T**, kinetic studies show otherwise. First, comparison of the LD spectra immediately after mixing of the complexes with DNA and at equilibrium reveal a slow change in binding mode with time for **T** while equilibrium is reached virtually instantly for **P**. Moreover, the dissociation rate differs significantly between the two complexes with **T** exhibiting very slow dissociation characteristic for threading intercalation. For **P**, on the other hand, it is difficult to judge whether the binding mode is classical or threading intercalation based on the dissociation rate constants (Table 4.3), which are just in between those for known classical and threading intercalating reference compounds. However, due to the larger hydrophobic surface of the phenyl-substituted dppz ligand the binding constant is expected to be larger for **P** than for $[Ru(phen)_2dppz]^{2+}$ which may account for the

Table 4.2. Roll angles for the ruthenium complexes bound to ct-DNA. A positive roll angle is defined as the clockwise rotation around the dppz long axis when looking along the dppz ligand from the ruthenium. A roll angle of 0° corresponds to the dppz short axis being oriented perpendicular to the DNA helix axis.

Complex	Δ	Λ
T	+4°	+14°
P	+9°	-2°
[Ru(phen) ₂ dppz] ²⁺	+7°	+13°

Table 4.3. Rate constants for SDS (0.6 %) induced dissociation of the ruthenium complexes from ct-DNA at 25 °C and 10 mM NaCl.

Complex	k_1 (10^{-2} s ⁻¹)	α_1	k_2 (10^{-2} s ⁻¹)	α_2
Δ - T	10	(0.33)	2.5	(0.67)
Λ - T	2.2	(0.38)	0.42	(0.62)
Δ - P	90	(0.59)	12	(0.41)
Λ - P	63	(0.56)	14	(0.44)
Δ -[Ru(phen) ₂ dppz] ²⁺	140			
Λ -[Ru(phen) ₂ dppz] ²⁺	890			

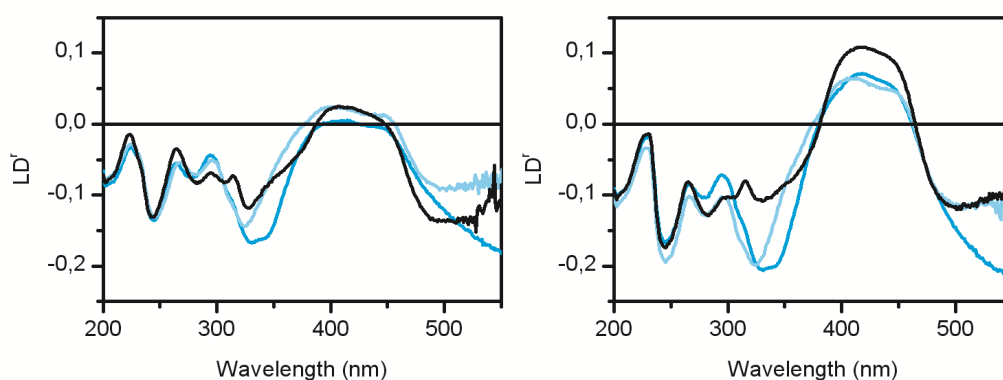


Figure 4.9. LD^r spectra of the Δ - (left) and Λ -enantiomers (right) of **T** (dark blue), **P** (light blue) and [Ru(phen)₂dppz]²⁺ (black) in presence of ct-DNA at equilibrium. The similar spectral shapes in the UV-region indicate similar binding geometries for all three complexes. The differences in the visible region are mainly due to differences in the isotropic absorption. Concentrations of complex, DNA and NaCl were 10, 120 and 10 μ M, respectively.

reduced dissociation rate of **P**. Therefore, the binding mode of **P** is proposed to be classical intercalation by insertion of part of the dppz ligand and one phenyl-substituent between the base pairs. In the threaded state envisioned for **T**, the dppz ligand is thought to be intercalated between the base pairs with both thienyl

substituents in the opposite groove relative to the ruthenium center. These two binding modes would give similar LD^r , since the LD^r is only sensitive to the angle between the transition dipole moments and the orientation axis, but explains the difference in association rates. Passage of the thienyl substituents through the base pair stack is likely to represent a significant energy barrier to reach the threaded state, and would account for the slow association and dissociation observed for **T**.

Considering the structural similarities of **P** and **T**, it is quite surprising that they have different binding modes. The distance between the outermost parts of the aryl-substituents is slightly larger for **P** than **T** (13.6 versus 12.6 Å as determined from PM3-optimized structures), and it is possible that **P** is too large while **T** is just small enough to pass through the base pair stack. This may explain why **P** does not thread DNA, but not why **T** does. A difference in stacking interactions between the aryl substituents and the DNA bases may explain the different binding modes. If the threading process is assumed to begin by insertion of one aryl-substituent between the base pairs, there must be a driving force for continued insertion of the ligand so that the dppz-part eventually becomes stacked between the base pairs with the aryl substituents in the groove. It is possible that the phenyl ring of **P** stacks very well with the bases so that there is no driving force for further insertion of the dppz ligand once the phenyl ring is intercalated, while the corresponding interactions are less favorable for the slightly thicker thienyl ring.

Previously it has been shown that the dissociation rate of threaded complexes is highly dependent on the charge of the bulky substituent that is passed through the base pair stack.¹¹⁹ Therefore, it is interesting to note that the dissociation rate constants for Λ -**T** are in the same range as those for mononuclear complexes with +1 charged ammonium-substituted dppz ligands. Hence, this work shows that the dissociation rate is also largely affected by the structure and position of the bulky substituents and that reduced charge on the bulky substituent can be compensated for by structural changes to retain the slow dissociation.

4.4 Thermodynamics and Cooperativity for Intercalating dppz Complexes

To date, all ruthenium complexes demonstrated to bind DNA by threading intercalation contain at least one dppz-moiety. Therefore, it is of great importance for this work to understand the interactions between the Ru-dppz structure and DNA. Binding of $[\text{Ru}(\text{phen})_2\text{dppz}]^{2+}$ and its analogue $[\text{Ru}(\text{bpy})_2\text{dppz}]^{2+}$ to DNA was proposed to occur by intercalation of the dppz ligand already in the first reports on their DNA interactions, but time-resolved emission studies revealed two emission lifetimes indicating two different modes of interaction.⁶³⁻⁶⁴ The origin of the two lifetimes has been subject to much research, but despite numerous publications on this matter consensus regarding the two lifetimes and the DNA binding mode has not been reached. Photophysical studies on enantiopure complexes with homogeneous polynucleotides ruled out sequence heterogeneity to be the cause of the two lifetimes and our lab proposed them to originate from

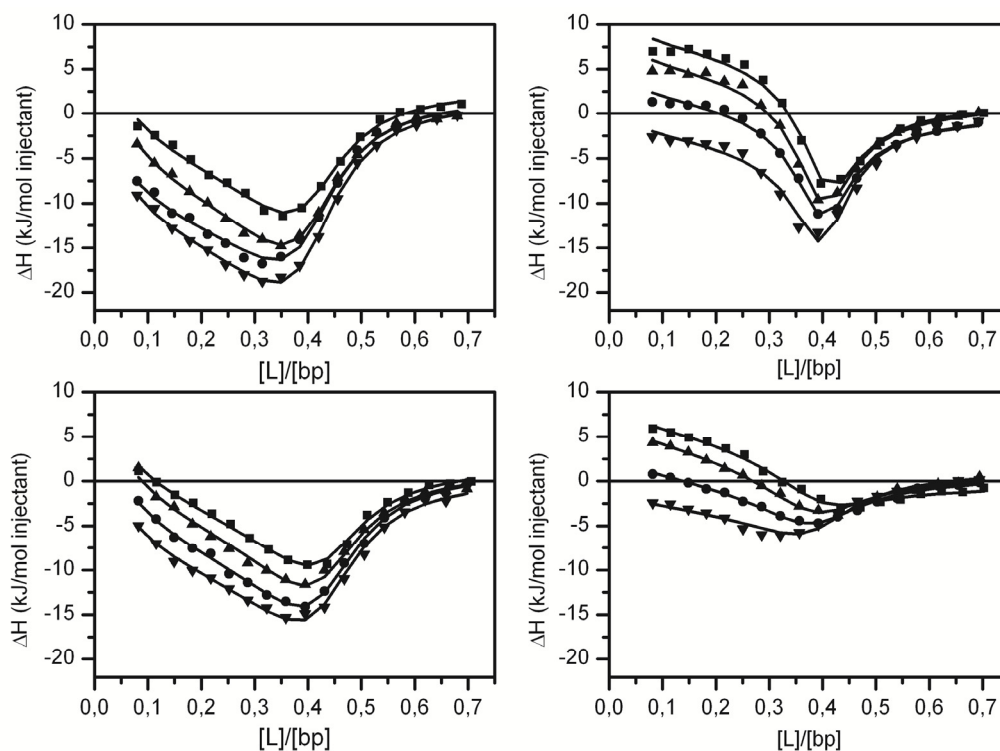


Figure 4.10. ITC data for titration of the Λ - (left) and Δ -enantiomers (right) of PHEN (top) and BPY (bottom) into AT-DNA (black) at 15 (■), 20 (▲), 25 (●) and 30 °C (▼). The solid lines are the simulated curves obtained when fitting the data with the binding model described below.

isolated and contiguously bound complexes in the minor groove.^{64, 92, 121} The Barton group, on the other hand, favored intercalation from the major groove with the two lifetimes being assigned to different intercalation geometries: one with the dppz ligand long axis centered in the intercalation pocket and one with a more canted geometry.^{85, 122-125} In Paper IV we have investigated the binding of enantiopure $[\text{Ru}(\text{phen})_2\text{dppz}]^{2+}$ (here denoted PHEN) and $[\text{Ru}(\text{bpy})_2\text{dppz}]^{2+}$ (BPY) to AT-DNA by isothermal titration calorimetry (ITC) and tried to correlate the ITC data to photophysical data to shed further light on the interactions between these complexes and DNA.

Figure 4.10 shows ITC data for titration of the four complexes into AT-DNA at 15, 20, 25 and 30 °C. The shape of the ITC profiles deviates strongly from standard ITC curves indicating that strong cooperativity effects are present. As the complex concentrations increase, binding of all four complexes gradually becomes more exothermic until a $[\text{Ru}]/[\text{bp}]$ ratio of approximately 0.3-0.4, but while the two Λ -complexes display similar ITC profiles, the differences to and between the Δ -enantiomers are striking. The signals for Δ -BPY are significantly smaller than for the other three complexes, and Δ -PHEN displays a plateau of constant heat

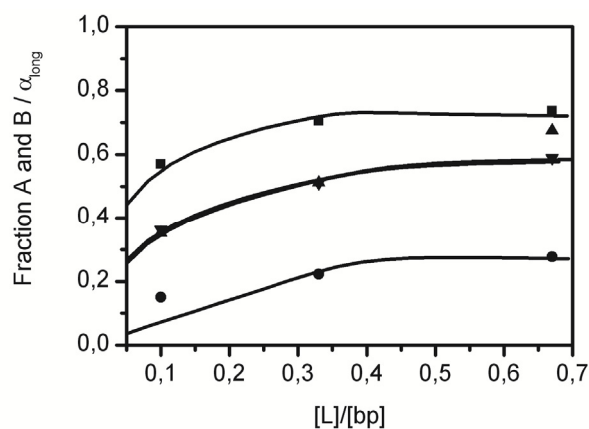


Figure 4.11. Pre-exponential factors for the long emission lifetimes of Δ -PHEN (■), Λ -PHEN (▲), Δ -BPY (●) and Λ -BPY (▼) at different binding ratios. The solid lines show the simulated fractions of species A and B obtained by fitting the data with the binding model described below. The data is nearly identical for the two Λ -enantiomers.

evolved for the first few injections with a more sharp decrease of the enthalpy compared with the other complexes. The shapes of the ITC profiles remain constant with varying temperature, but the reactions become more exothermic as the temperature increases.

To correlate the ITC data with previous photophysical studies, emission lifetime measurements were performed at three binding ratios: $[L]/[bp] = 0.1, 0.33$ and 0.67 corresponding to the low, middle and high saturation regimes respectively. The pre-exponential factor for the long emission lifetime, α_{long} increases with binding ratio for all complexes, but again there are significant differences between the Δ -enantiomers while the two Λ -enantiomers display similar trends. α_{long} is substantially smaller for Δ -BPY at all binding ratios compared with the Λ -enantiomers, whereas Δ -PHEN displays significantly larger values (Figure 4.11).

The simplest model that can satisfactorily fit both ITC and emission lifetime data includes two bound species with different binding geometries to account for the two emission lifetimes, one of which is polar to allow both cooperative and anti-cooperative interactions between the two (Figure 4.12). The polar species is denoted A or B depending on the polarity, and the symmetrical species is denoted C. For symmetry reasons, we assign species C and A/B to a centered and a canted intercalation geometry respectively, as proposed by Barton and co-workers,⁸⁵ but contrary to the original proposal we attribute the long emission lifetime to the canted geometry. This is based on the fact that the emission lifetime of dppz complexes depends on whether only one or both phenazine nitrogens are accessible for water.⁸⁷ If intercalation occurs from the minor groove, this would presumably result in one nitrogen being fully and the other one partly protected

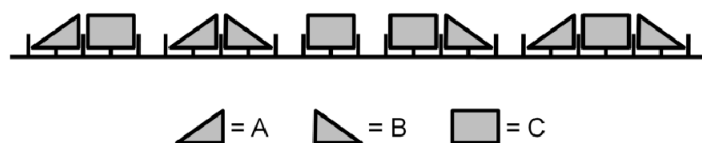


Figure 4.12. Schematic picture illustrating the binding model with polar species A and B and the non-polar species C.

from water in the in the canted geometry, which would result in quenching being less probable than for the centered geometry where both nitrogens are thought to be partly accessible to water.

As a consequence of α_{long} approaching zero at low binding ratios (unpublished data at 10 mM NaCl, Lincoln and Tuite) complexes only exist as A/B when they are bound in close contact with another complex, implying that isolated complexes only exist in geometry C. Further, many of the theoretically possible combinations of complex-complex interactions have been excluded from the model for sterical reasons as complexes canted towards each other would clash. Only the complex-complexes interactions AB, AC/CB and CC are allowed, which means that A/B are present only at the ends of contiguous sequences and only the centered C can be accommodated in the interior of such. In addition to the intrinsic binding enthalpy, which is assumed to be the same regardless if the complexes are isolated or contiguously bound, complex-complex interactions for the combinations AC/CB and CC are thought to give rise to an additional interaction enthalpy. The parameter values that gave the best fit to both ITC data and the α_{long} -values (solid lines in Figure 4.10 and 4.11) are presented in Table 4.4 along with thermodynamic data for the intrinsic binding obtained at 20 °C in Table 4.5.

Although the numbers presented in Table 4.4 should be interpreted with caution since the parameters in the model are not all independent and better fits may be obtained by more complicated models, several qualitative conclusions regarding the DNA binding of the studied complexes can be made. Overall, Δ -BPY appears to be most anti-cooperative since all complex-complex interactions are anti-cooperative, in contrast to the binding of the other complexes which appear to be moderately cooperative. The CC interaction is anti-cooperative for all complexes, suggesting that they are reluctant to form longer contiguous sequences than three complexes in a row. The AB combination, where the complexes are canted away from each other, is strongly favored for Δ -PHEN. Thus, the exothermic enthalpy observed close to saturation can mainly be ascribed to AB-duplets forming ACB-triplets. A similar interpretation will hold also for the Λ -complexes. We propose that steric and/or electrostatic repulsion between the phenanthroline or bipyridine ligands account for the anti-cooperativity when complexes are closely packed, whereas we believe that the cooperativity observed for complexes canted away from their neighbor is an effect of allosteric widening of the groove and favourable interactions between the phenantrolines/bipyridines and the DNA.

Table 4.4. Intrinsic binding constants K , cooperativity parameters y , and binding site sizes n for binding of dppz complexes to AT-DNA.

Complex	K (10^6 M^{-1})	y_{AB}	$y_{AC/CB}$	y_{CC}	$n_{A/B}$	n_c
Δ -PHEN	1.1	56	6	0.01	2	1.8
Δ -BPY	1.3	0.3	0.6	0.2	2	1.8
Λ -PHEN	0.2	8	9	0.05	2	1.8
Λ -BPY	0.2	10	9	0.05	1.85	1.65

Table 4.5. Thermodynamic data for the intrinsic binding at 20 °C.

Complex	ΔG (kJ mol^{-1})	ΔH (kJ mol^{-1})	ΔS ($\text{J K}^{-1} \text{ mol}^{-1}$)	ΔC_p ($\text{J K}^{-1} \text{ mol}^{-1}$)
Δ - PHEN	-33.9	7.4	140	-570
Δ - BPY	-34.3	4.5	130	-670
Λ - PHEN	-29.8	7.2	130	-450
Λ -BPY	-29.8	10.9	140	-310

Comparison of the relative contributions of ΔH and ΔS to ΔG in Table 4.5 shows that the intrinsic binding is entropically driven. This indicates that desolvation of hydrophobic surfaces play an important role for binding affinity, which is also supported by the negative ΔC_p . Altogether, these results clearly show that complex-complex interactions have great influence on the intercalation of dppz-complexes into AT-DNA and it is likely that these effects are present also for threading intercalating complexes. Cooperativity may explain the slow redistribution of threaded complexes along the DNA polymer and the observation of bi-exponential dissociation kinetic traces.⁷³⁻⁷⁵

Figure 4.13 shows a comparison of ITC data for Δ -PHEN titrated into AT- and ct-DNA at 25 °C. It appears from Figure 4.13 that intercalation is more endothermic and the cooperativity less pronounced for ct-DNA, which is consistent with the previous report by Haq et al.¹²⁶ A more endothermic interaction enthalpy may, at least partly, explain the lower affinity for ct-DNA compared with AT-DNA, and the absence of the strong exothermic enthalpy close to saturation suggests that the complexes are not as densely packed on ct-DNA. Although the data presented in Figure 4.13 is only preliminary, it clearly shows that the complex-complex interactions of Δ -PHEN differs depending on the type of DNA. Such interactions in the bound state may be of importance also for threading intercalation ruthenium complexes, and may contribute to the AT-selectivity of these compounds.

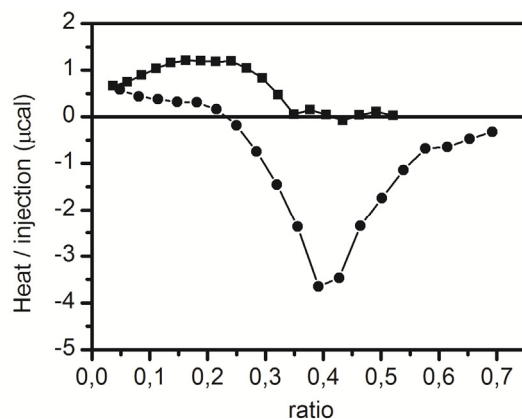


Figure 4.13. ITC data for titration of Δ -PHEN into ct- (■) and AT-DNA (●) at 25 °C.

4.5 Cell Localization and Uptake

All the DNA studies discussed above have been performed in simple systems containing only DNA and ruthenium complex in sodium chloride solution, and due to the relatively few cell studies on binuclear ruthenium polypyridyl complexes little is known about their interactions with cells.^{67, 71, 127-129} Therefore, if the complexes are to be of any biological interest, it is of great importance to investigate how the complexes behave inside cells where they encounter a much more complex milieu due to the presence of other biomolecules. For this work it is of particular importance to confirm that DNA binding can occur inside cells, but from a more general point of view it is also interesting to investigate other aspects of the interactions with living cells, such as uptake and toxicity.

Since both the *meta*- and *para*-isomers of **2** (here denoted **m** and **p**) are highly luminescent in both polar and non-polar environments and their quantum yields are rather insensitive to the environment, these complexes are suitable as model compounds for studies of cellular uptake and localization of binuclear ruthenium complexes. Figure 4.14 shows confocal laser scanning microscopy images of cells that have been incubated 1 h with 5 μ M $\Delta\Delta$ -**m**. As seen by the punctuate staining of the cytosol, the complex is readily internalized already at this low concentration and the uptake mechanism is probably endocytosis as the complex appears to be localized in endosomes. An endocytotic uptake mechanism is further supported by the fact that no uptake was observed when the same experiment was performed at 4°C, where energy dependent mechanisms such as endocytosis are inhibited. Experiments on the other isomers yielded similar results. Uptake via endocytosis has previously been observed for $[\mu\text{-C4}(\text{cpdppz})_2(\text{phen})_4\text{Ru}_2]^{4+}$,¹²⁷ but other mechanisms has been proposed for other binuclear ruthenium complexes.^{71, 128} Co-staining with the dead cell marker Sytox Green showed that the concentrations used for the uptake studies are non-toxic to the cells, and it should also be noted

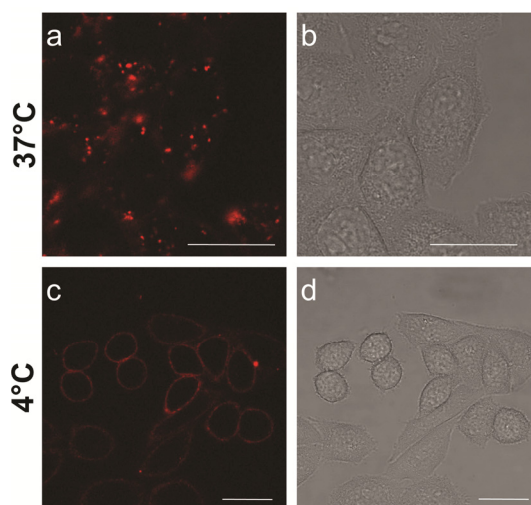


Figure 4.14. Representative confocal laser scanning microscopy images of live CHO-K1 cells after 1 h incubation with $\Delta\Delta\text{-m}$ ($5\ \mu\text{M}$) at a) $37\ ^\circ\text{C}$ and c) $4\ ^\circ\text{C}$. b) and d) are the corresponding transmission images. Scale bars are $20\ \mu\text{m}$.

that these concentrations are significantly lower than the ones used for cell staining with other binuclear ruthenium complexes.^{71, 128-129}

The cellular localization of the complexes was also investigated in fixed cells, where the cell membrane has been permeabilized with cold methanol to allow free passage of the complexes into the cytosol. As seen in Figure 4.15, the staining pattern in fixed cells is very different from that in live cells for all four isomers, indicating that the staining of the endosomes in live cells is due to difficulties for the complexes to escape the membrane enclosed vesicles rather than an actual preference for them. The affinity for various cellular components appears, at least for the investigated complexes, to be more sensitive to the chirality around the ruthenium center than complex structure, with the $\Delta\Delta$ -enantiomers displaying intense emission inside the nucleus while the $\Lambda\Lambda$ -enantiomers stain the cytosol and the nucleoli. This shows that chirality is an important factor to consider when designing molecules targeting cellular components. Both enantiomers also bind to membrane structures, but these interactions seem to be less sensitive to chirality.

Cell studies have also been performed for $\Delta\Delta\text{-1}$, $\Delta\Lambda\text{-3}$ and $\Delta\Delta\text{-4}$ to investigate whether threading intercalation occurs also in cells. None of the complexes could be detected inside live cells after 1 h incubation with $5\ \mu\text{M}$ complex, but in resemblance with the other binuclear complexes they are probably taken up via endocytosis and trapped in endosomes where they are not emissive. After addition of methanol to the cells, which kills them and also permeabilizes the endosome membranes, staining of the cells slowly appears (Figure 4.16). The effect is most pronounced for $\Delta\Delta\text{-4}$, which after 3 h at 37°C stains the nucleus and nucleoli, indicating that $\Delta\Delta\text{-4}$ binds DNA and perhaps also RNA by threading intercalation.

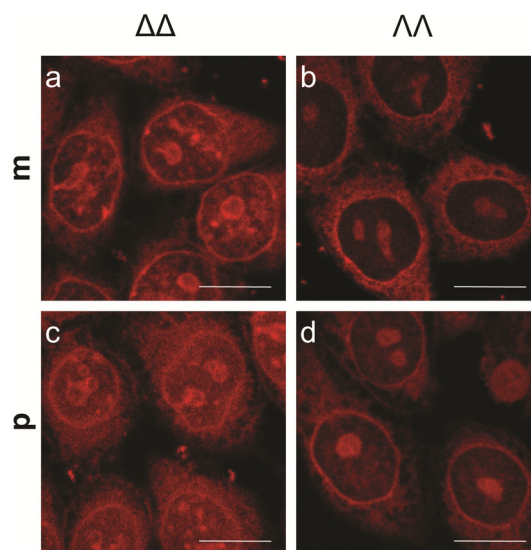


Figure 4.15. Representative confocal laser scanning microscopy images of a) $\Delta\Delta$ -**m**, b) $\Lambda\Lambda$ -**m**, c) $\Delta\Delta$ -**p**, and d) $\Lambda\Lambda$ -**p** in fixed cells. Cells were fixed with methanol (-20°C , 15 min) and incubated 4 h with $5\ \mu\text{M}$ ruthenium complex before imaging. Scale bars are $10\ \mu\text{m}$.

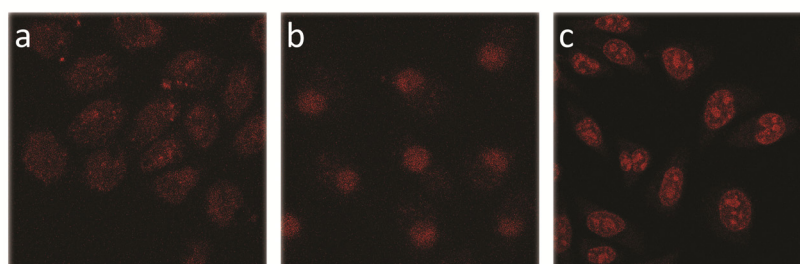


Figure 4.16. Confocal laser scanning microscopy images of a) $\Delta\Delta$ -**1**, b) $\Delta\Delta$ -**3** and c) $\Delta\Delta$ -**4** in dead cells. Live cells were incubated 1 h with $5\ \mu\text{M}$ complex, and then rinsed once before a few drops of MeOH was added to kill the cells. Staining of the cells appeared slowly, and images were taken after approximately 3 h incubation at 37°C .

$\Delta\Delta$ -**3** exhibits a similar staining pattern, but the intensity is much weaker, which could be due to that threading of **3** is much slower and more AT-selective compared with **4**. Surprisingly, $\Delta\Delta$ -**1** displays a more diffuse staining than the other two complexes, where emission is detected also in the cytosol. The intensity is very weak also for $\Delta\Delta$ -**1**. Similar results were obtained when adding complex to already fixed cells, except that $\Delta\Delta$ -**3** now displays a more diffuse staining. Although these are only preliminary results, they show that threading intercalation probably is possible also in cells, but that the reaction is very slow as expected. In resemblance with **2**, uptake appears to occur via endocytosis, and endosomal escape may be a potential problem that has to be solved for any biological use.

5 CONCLUDING REMARKS

In this thesis the DNA binding properties of several new ruthenium complexes have been investigated, which has resulted in the discovery of three new threading intercalators: $[\mu\text{-dppzip}(\text{phen})_4\text{Ru}_2]^{4+}$, $[\mu\text{-bidppze}(\text{phen})_4\text{Ru}_2]^{4+}$ and $[\text{Ru}(\text{phen})_2\text{-10,13-di}(2'\text{-thienyl)dppz}]^{2+}$. Comparison of the new binuclear complexes with the previously studied $[\mu\text{-bidppz}(\text{phen})_4\text{Ru}_2]^{4+}$ has led to several conclusions regarding the effect of complex structure on threading intercalation ability. In particular it has been shown that a shorter bridging ligand results in increased AT-selectivity but reduced binding constant, whereas elongation of the bridging ligand has the opposite effects. Studies on the four stereoisomers of $[\mu\text{-dppzip}(\text{phen})_4\text{Ru}_2]^{4+}$ revealed Δ -conformation on the dppz-half and Λ -conformation on the ip-half to be the optimal geometries, showing that the structural requirements are different for the two grooves. The fact that the two structural isomers of $[\mu\text{-bipb}(\text{phen})_4\text{Ru}_2]^{4+}$ do not bind DNA by threading intercalation suggests that increased flexibility is not beneficial for this type of binding, though it should be kept in mind that the bipb complexes have smaller aromatic ring systems than the dppz complexes which could make intercalation less favorable for the former ones. To date, all reported threading intercalating ruthenium complexes contain at least one dppz-moiety, suggesting that this structure plays an important role for the DNA interaction.

Despite these new insights regarding the structural requirements for threading intercalation of binuclear ruthenium complexes there is still much to learn to fully understand this type of binding. Considering the structural diversity of known threading intercalators (Figure 2.4) it would be interesting to do more systematic studies also on other types of threading compounds in order to generalize the results. For example, $[\mu\text{-dppzip}(\text{phen})_4\text{Ru}_2]^{4+}$ appears to be just at the border of being capable of threading intercalation with dissociation rate constants significantly larger than for the parent complex $[\mu\text{-bidppz}(\text{phen})_4\text{Ru}_2]^{4+}$, which is thought to be an effect of the shorter bridging ligand. Yet, nogalamycin, where the distance between the bulky substituents is even shorter, displays dissociation rates comparable to those of $[\mu\text{-bidppz}(\text{phen})_4\text{Ru}_2]^{4+}$ suggesting that there are other factors than just bridging ligand length involved.⁶⁻⁷

One of the new complexes, $[\mu\text{-dppzip}(\text{phen})_4\text{Ru}_2]^{4+}$, display a remarkable AT-selectivity, which is promising for targeting AT-rich DNA, for example in parasites. However, in order to target specific genes the selectivity has to be increased even further. A possible strategy to achieve this and still maintain the slow dissociation

could be to attach sequence recognizing moieties, such as the hairpin polyamides developed by Dervan and co-workers,^{20, 23-24} to threading intercalating complexes. An advantage of threading intercalating compounds compared with other synthetic DNA binders is that the minor groove can be used for gene recognition to block DNA interactions also in the major groove. There are examples in the literature where oligonucleotides and peptides have been attached to dppz and bipyridine ligands of ruthenium complexes, respectively, showing that there are synthetic methods to attach such moieties to polypyridyl ligands.^{120, 130-133} Grimm et al. have also reported sequence specific threading intercalation into duplex DNA by triplex formation of oligonucleotide tethered $[\text{Ru}(\text{phen})_2\text{dppz}]^{2+}$.¹²⁰

Studies on dead cells with permeabilized membranes show that threading occurs also in the complex milieu inside cells demonstrating the biological relevance of these complexes. However, in live cells the complexes appear to be internalized via endocytosis where they remain trapped in the endosomes, which is a problem that needs to be addressed if the complexes are to be used for any biological applications. Nuclear localization could be enhanced by attachment of peptide constructs to the complexes as previously described by Barton and co-workers.¹³¹⁻¹³² Also, increased lipophilicity of the complexes may enhance membrane penetration.¹³⁴⁻¹³⁶ For this purpose, the mononuclear 10,13-substituted dppz complexes may serve as a starting point for design of new threading intercalators with reduced charge, as studies on this type of complexes have shown that reduced charge can be compensated for by structural changes to maintain the slow dissociation. Although all three binuclear threading complexes stain the nucleus as expected for DNA binding compounds, $[\mu\text{-dppzip}(\text{phen})_4\text{Ru}_2]^{4+}$ and $[\mu\text{-bidppze}(\text{phen})_4\text{Ru}_2]^{4+}$ display distinct staining also of the nucleoli while $[\mu\text{-bidppz}(\text{phen})_4\text{Ru}_2]^{4+}$ displays diffuse staining of the cytosol. Thus, the complexes appear to interact also with other cellular components than DNA, showing that there is a need to further investigate the preference for DNA in comparison with other biomolecules such as RNA to fully understand the factors controlling selectivity.

The rare and charged ruthenium ion may seem as an odd choice for development of DNA binding molecules for therapeutical purposes. However, the primary goal of this thesis has not been to develop drugs ready for therapeutical use but to increase the understanding of the relationship between molecular structure and threading intercalation properties. For this purpose ruthenium is an excellent choice since it enables systematic variations of the structure and the resulting complexes are stable and easily obtained in their pure enantiomeric forms. The results show the potential of threading intercalating compounds as sequence specific DNA binding drugs and the new insights regarding the structural requirements for this type of binding may hopefully contribute to design of new and better threading compounds in the future. The ruthenium ions could for example be substituted for the more abundant iron ion or a monovalent metal to reduce the charge. Metal-free compounds with protonated groups such as amines

is also a possibility. Recently, two ruthenium anticancer agents have reached clinical trials.⁶⁶ Although these complexes are structurally very different from the ones studied here, this shows that the idea of ruthenium based drugs is not so far-fetched after all, motivating further studies also on ruthenium complexes. The AT-specific $[\mu\text{-dppzip}(\text{phen})_4\text{Ru}_2]^{4+}$ is particularly interesting in the context of parasite diseases, but it should be kept in mind that there are many other factors in addition to the DNA binding properties that determine the therapeutical use of a compound.

6 ACKNOWLEDGEMENTS

I would like to express my gratitude to the following people who has contributed, in one way or another, to complete this thesis:

My supervisor PER for excellent guidance, patience and encouragement. I know these last six months have been tough for you, but still you have always had time for me. I really appreciate it! • My co-supervisor JOCKE – I really enjoyed and learnt a lot from working with the spiropyrans. • BENGT for funding and for letting me be part of the Nordén Group. • My co-authors MINNA, PÅR, LOUISE, MARIA A, EIMER, FRIDA, HELENE, MARTIN and SHIMING for great collaborations. • PÅR for introducing me to the project and giving me a good start. • HELENE for always keeping an eye on me and for great collaboration with the bachelor projects which lead the research into a more biological direction. • FRIDA for all the good advice during the years and for completing the cell studies. • MARIA A for taking on the role as my “mentor” during thesis writing. • FREDRIK and MARIA A for proofreading the thesis. • MINNA for helping me out in the synthesis lab. • JOHAN who also helped with synthesis. • MARTIN and YUBO for excellent master thesis work – I learnt a lot from working with you and I hope you did too. • All BACHELOR STUDENTS who did the lab work I didn't have time do myself. • Former and present COLLEGUES at Physical Chemistry for the nice atmosphere in the fika-room. • FAMILY and FRIENDS for always being there!

7 REFERENCES

1. Landry, Y., Gies, J. P., Drugs and Their Molecular Targets: An Updated Overview. *Fundam. Clin. Pharmacol.* **2008**, *22* (1), 1-18.
2. Latchman, D. S., How Can We Use Our Growing Understanding of Gene Transcription to Discover Effective New Medicines? *Curr. Opin. Biotechnol.* **1997**, *8* (6), 713-717.
3. Winters, T. A., Gene Targeted Agents: New Opportunities for Rational Drug Development. *Curr. Opin. Mol. Ther.* **2000**, *2* (6), 670-681.
4. Lander, E. S., Linton, L. M., Birren, B., *et al.*, Initial Sequencing and Analysis of the Human Genome. *Nature* **2001**, *409* (6822), 860-921.
5. Watson, J. D., Crick, F. H. C., Molecular Structure of Nucleic Acids - a Structure for Deoxyribose Nucleic Acid. *Nature* **1953**, *171* (4356), 737-738.
6. Fox, K. R., Waring, M. J., Evidence of Different Binding-Sites for Nogalamycin in DNA Revealed by Association Kinetics. *Biochim. Biophys. Acta* **1984**, *802* (2), 162-168.
7. Fox, K. R., Brassett, C., Waring, M. J., Kinetics of Dissociation of Nogalamycin from DNA - Comparison with Other Anthracycline Antibiotics. *Biochim. Biophys. Acta* **1985**, *840* (3), 383-392.
8. Collier, D. A., Neidle, S., Brown, J. R., Molecular Models for the Interaction of the Anti-Tumor Drug Nogalamycin with DNA. *Biochem. Pharmacol.* **1984**, *33* (18), 2877-2880.
9. Nordell, P., Westerlund, F., Wilhelmsson, L. M., *et al.*, Kinetic Recognition of AT-Rich DNA by Ruthenium Complexes. *Angew. Chem., Int. Ed.* **2007**, *46* (13), 2203-2206.
10. Bloomfield, V. A., Crothers, D. M., Tinoco, I., *Nucleic Acids. Structures, Properties and Functions*. University Science Books: Sausalito, 2000.
11. Ussery, D. W., DNA Structure: A-, B- and Z-DNA Helix Families. In: *Encyclopedia of Life Sciences*, John Wiley & Sons Ltd, Chichester, 2002, <http://www.els.net/>.
12. Alberts, B., Johnson, A., Lewis, J., *et al.*, *Molecular Biology of the Cell*. Taylor & Francis Inc.: New York, 2002.
13. Benson, M. D. Amyloidosis. In: *Encyclopedia of Life Sciences*, John Wiley & Sons Ltd, Chichester, 2008, <http://www.els.net/>.
14. Vazquez, M. E., Caamano, A. M., Mascarenas, J. L., From Transcription Factors to Designed Sequence-Specific DNA-Binding Peptides. *Chem. Soc. Rev.* **2003**, *32* (6), 338-349.
15. Grzeskowiak, K., Sequence-Dependent Structural Variation in B-DNA. *Chem. Biol.* **1996**, *3* (10), 785-790.

16. Chaney, S. G., Sancar, A., DNA Repair: Enzymatic Mechanisms and Relevance to Drug Response. *J. Natl. Cancer Inst.* **1996**, *88* (19), 1346-1360.
17. Hurley, L. H., DNA and Its Associated Processes as Targets for Cancer Therapy. *Nat. Rev. Cancer* **2002**, *2* (3), 188-200.
18. Shewach, D. S., Kuchta, R. D., Introduction to Cancer Chemotherapeutics. *Chem. Rev.* **2009**, *109* (7), 2859-2861.
19. Thuong, N. T., Helene, C., Sequence-Specific Recognition and Modification of Double-Helical DNA by Oligonucleotides. *Angew. Chem., Int. Ed. Engl.* **1993**, *32* (5), 666-690.
20. Trauger, J. W., Baird, E. E., Dervan, P. B., Recognition of 16 Base Pairs in the Minor Groove of DNA by a Pyrrole-Imidazole Polyamide Dimer. *J. Am. Chem. Soc.* **1998**, *120* (14), 3534-3535.
21. Lerman, L. S., Structural Considerations in Interaction of DNA and Acridines. *J. Mol. Biol.* **1961**, *3* (1), 18-30.
22. Seeman, N. C., Rosenberg, J. M., Rich, A., Sequence-Specific Recognition of Double Helical Nucleic-Acids by Proteins. *Proc. Natl. Acad. Sci. U.S.A.* **1976**, *73* (3), 804-808.
23. White, S., Szewczyk, J. W., Turner, J. M., *et al.*, Recognition of the Four Watson-Crick Base Pairs in the DNA Minor Groove by Synthetic Ligands. *Nature* **1998**, *391* (6666), 468-471.
24. Dervan, P. B., Edelson, B. S., Recognition of the DNA Minor Groove by Pyrrole-Imidazole Polyamides. *Curr. Opin. Struct. Biol.* **2003**, *13* (3), 284-299.
25. Dickinson, L. A., Gulizia, R. J., Trauger, J. W., *et al.*, Inhibition of RNA Polymerase II Transcription in Human Cells by Synthetic DNA-Binding Ligands. *Proc. Natl. Acad. Sci. U.S.A.* **1998**, *95* (22), 12890-12895.
26. Ehley, J. A., Melander, C., Herman, D., *et al.*, Promoter Scanning for Transcription Inhibition with DNA-Binding Polyamides. *Mol. Cell. Biol.* **2002**, *22* (6), 1723-1733.
27. Dickinson, L. A., Burnett, R., Melander, C., *et al.*, Arresting Cancer Proliferation by Small-Molecule Gene Regulation. *Chem. Biol.* **2004**, *11* (11), 1583-1594.
28. Wheate, N. J., Brodie, C. R., Collins, J. G., *et al.*, DNA Intercalators in Cancer Therapy: Organic and Inorganic Drugs and Their Spectroscopic Tools of Analysis. *Mini-Rev. Med. Chem.* **2007**, *7* (6), 627-648.
29. Bischoff, G., Hoffmann, S., DNA-Binding of Drugs Used in Medicinal Therapies. *Curr. Med. Chem.* **2002**, *9* (3), 321-348.
30. Wilson, W. D., Tanious, F. A., Mathis, A., *et al.*, Antiparasitic Compounds That Target DNA. *Biochimie* **2008**, *90* (7), 999-1014.
31. Wilson, W. D., Nguyen, B., Tanious, F. A., *et al.*, Dications That Target the DNA Minor Groove: Compound Design and Preparation, DNA Interactions, Cellular Distribution and Biological Activity. *Curr. Med. Chem.* **2005**, *5*, 389-408.
32. Paramanathan, T., Westerlund, F., McCauley, M. J., *et al.*, Mechanically Manipulating the DNA Threading Intercalation Rate. *J. Am. Chem. Soc.* **2008**, *130* (12), 3752-3753.
33. Tanious, F. A., Yen, S. F., Wilson, W. D., Kinetic and Equilibrium-Analysis of a Threading Intercalation Mode - DNA-Sequence and Ion Effects. *Biochemistry* **1991**, *30* (7), 1813-1819.
34. Wakelin, L. P. G., Bu, X. Y., Eleftheriou, A., *et al.*, Bisintercalating Threading Diacridines: Relationships between DNA Binding, Cytotoxicity, and Cell Cycle Arrest. *J. Med. Chem.* **2003**, *46* (26), 5790-5802.

35. Önfelt, B., Lincoln, P., Norden, B., Enantioselective DNA Threading Dynamics by Phenazine-Linked [Ru(phen)₂dppz]²⁺ Dimers. *J. Am. Chem. Soc.* **2001**, *123* (16), 3630-3637.
36. Önfelt, B., Lincoln, P., Norden, B., A Molecular Staple for DNA: Threading Bis-Intercalating [Ru(phen)₂dppz]²⁺ Dimer. *J. Am. Chem. Soc.* **1999**, *121* (46), 10846-10847.
37. Holman, G. G., Zewail-Foote, M., Smith, A. R., *et al.*, Sequence-Specific Threading Tetra-Intercalator with an Extremely Slow Dissociation Rate Constant. *Nat. Chem.* **2011**, *3* (11), 875-881.
38. Guelev, V., Lee, J., Ward, J., *et al.*, Peptide Bis-Intercalator Binds DNA Via Threading Mode with Sequence Specific Contacts in the Major Groove. *Chem. Biol.* **2001**, *8* (5), 415-425.
39. Kersten, W., Kersten, H., Szybalski, W., Physicochemical Properties of Complexes between Deoxyribonucleic Acid and Antibiotics Which Affect Ribonucleic Acid Synthesis. *Biochemistry* **1966**, *5* (1), 236-244.
40. Smith, C. K., Davies, G. J., Dodson, E. J., *et al.*, DNA-Nogalamycin Interactions - the Crystal-Structure of d(TGATCA) Complexed with Nogalamycin. *Biochemistry* **1995**, *34* (2), 415-425.
41. Muller, W., Crothers, D. M., Studies of Binding of Actinomycin and Related Compounds to DNA. *J. Mol. Biol.* **1968**, *35* (2), 251-290.
42. Feigon, J., Denny, W. A., Leupin, W., *et al.*, Interactions of Antitumor Drugs with Natural DNA - ¹H-NMR Study of Binding Mode and Kinetics. *J. Med. Chem.* **1984**, *27* (4), 450-465.
43. Wakelin, L. P. G., Waring, M. J., Kinetics of Drug-DNA Interaction - Dependence of the Binding Mechanism on Structure of the Ligand. *J. Mol. Biol.* **1980**, *144* (2), 183-214.
44. Zhao, M., Janda, L., Nguyen, J., *et al.*, The Interaction of Substituted 2-Phenylquinoline Intercalators with Poly(A).Poly(U) - Classical and Threading Intercalation Modes with RNA. *Biopolymers* **1994**, *34* (1), 61-73.
45. Ohtsuka, K., Komizo, K., Takenaka, S., Synthesis and DNA Binding Behavior of a Naphthalene Diimide Derivative Carrying Two Dicobalt Hexacarbonyl Complexes as an Infrared DNA Probe. *J. Organomet. Chem.* **2010**, *695* (9), 1281-1286.
46. Sato, S., Hirano, A., Takenaka, S., Selective Immobilization of Double Stranded DNA on a Gold Surface through Threading Intercalation of a Naphthalene Diimide Having Dithiolane Moieties. *Anal. Chim. Acta* **2010**, *665* (1), 91-97.
47. Sato, S., Nojima, T., Waki, M., *et al.*, Supramolecular Complex Formation by Beta-Cyclodextrin and Ferrocenyl-naphthalene Diimide-Intercalated Double Stranded DNA and Improved Electrochemical Gene Detection. *Molecules* **2005**, *10* (6), 693-707.
48. Sato, S., Tsueda, M., Takenaka, S., Electrochemical Detection of Aberrant Methylated Gene Using Naphthalene Diimide Derivative Carrying Four Ferrocene Moieties. *J. Organomet. Chem.* **2010**, *695* (15-16), 1858-1862.
49. Bourdouxhe-Housiaux, C., Colson, P., Houssier, C., *et al.*, Interaction of a DNA-Threading Netropsin-Amsacrine Combilexin with DNA and Chromatin. *Biochemistry* **1996**, *35* (14), 4251-4264.
50. Carlson, C. B., Vuyisich, M., Gooch, B. D., *et al.*, Preferred RNA Binding Sites for a Threading Intercalator Revealed by in Vitro Evolution. *Chem. Biol.* **2003**, *10* (7), 663-672.
51. Gooch, B. D., Beal, P. A., Recognition of Duplex RNA by Helix-Threading Peptides. *J. Am. Chem. Soc.* **2004**, *126* (34), 10603-10610.

52. Gooch, B. D., Krishnamurthy, M., Shadid, M., *et al.*, Binding of Helix-Threading Peptides to E-Coli 16S Ribosomal RNA and Inhibition of the S15-16S Complex. *ChemBioChem* **2005**, *6* (12), 2247-2254.
53. Krishnamurthy, M., Gooch, B. D., Beal, P. A., RNA Binding and Thiolytic Stability of a Quinoline-Containing Helix-Threading Peptide. *Org. Biomol. Chem.* **2006**, *4* (4), 639-645.
54. Fedoroff, O. Y., Salazar, M., Han, H. Y., *et al.*, NMR-Based Model of a Telomerase-Inhibiting Compound Bound to G-Quadruplex DNA. *Biochemistry* **1998**, *37* (36), 12367-12374.
55. Haq, I., Trent, J. O., Chowdhry, B. Z., *et al.*, Intercalative G-Tetraplex Stabilization of Telomeric DNA by a Cationic Porphyrin. *J. Am. Chem. Soc.* **1999**, *121* (9), 1768-1779.
56. Tanious, F. A., Jenkins, T. C., Neidle, S., *et al.*, Substituent Position Dictates the Intercalative DNA-Binding Mode for Anthracene-9,10-Dione Antitumor Drugs. *Biochemistry* **1992**, *31* (46), 11632-11640.
57. Martelli, A., Jourdan, M., Constant, J. F., *et al.*, Photoreactive Threading Agent That Specifically Binds to Abasic Sites in DNA. *Bioorg. Med. Chem. Lett.* **2006**, *16* (1), 154-157.
58. Kogan, M., Norden, B., Lincoln, P., *et al.*, Transition State of Rare Event Base Pair Opening Probed by Threading into Looped DNA. *ChemBioChem* **2011**, *12* (13), 2001-2006.
59. Barton, J. K., Danishefsky, A. T., Goldberg, J. M., Tris(phenanthroline)Ruthenium(II) - Stereoselectivity in Binding to DNA. *J. Am. Chem. Soc.* **1984**, *106* (7), 2172-2176.
60. Erkkila, K. E., Odom, D. T., Barton, J. K., Recognition and Reaction of Metallo-intercalators with DNA. *Chem. Rev.* **1999**, *99* (9), 2777-2795.
61. Metcalfe, C., Thomas, J. A., Kinetically Inert Transition Metal Complexes That Reversibly Bind to DNA. *Chem. Soc. Rev.* **2003**, *32* (4), 215-224.
62. Vos, J. G., Kelly, J. M., Ruthenium Polypyridyl Chemistry, from Basic Research to Applications and Back Again. *Dalton Trans.* **2006**, (41), 4869-4883.
63. Friedman, A. E., Chambron, J. C., Sauvage, J. P., *et al.*, Molecular Light Switch for DNA - Ru(bpy)₂(dppz)²⁺. *J. Am. Chem. Soc.* **1990**, *112* (12), 4960-4962.
64. Hiort, C., Lincoln, P., Norden, B., DNA-Binding of Δ -[Ru(phen)₂dppz]²⁺ and Λ -[Ru(phen)₂dppz]²⁺. *J. Am. Chem. Soc.* **1993**, *115* (9), 3448-3454.
65. Keene, F. R., Smith, J. A., Collins, J. G., Metal Complexes as Structure-Selective Binding Agents for Nucleic Acids. *Coord. Chem. Rev.* **2009**, *253* (15-16), 2021-2035.
66. Antonarakis, E. S., Emadi, A., Ruthenium-Based Chemotherapeutics: Are They Ready for Prime Time? *Cancer Chemother. Pharmacol.* **2010**, *66* (1), 1-9.
67. Salassa, L., Polypyridyl Metal Complexes with Biological Activity. *Eur. J. Inorg. Chem.* **2011**, (32), 4931-4947.
68. Bhat, S. S., Kumbhar, A. S., Kumbhar, A. A., *et al.*, Ruthenium(II) Polypyridyl Complexes as Carriers for DNA Delivery. *Chem. Commun.* **2011**, *47* (39), 11068-11070.
69. Musatkina, E., Amouri, H., Lamoureux, M., *et al.*, Mono- and Dicarboxylic Polypyridyl-Ru Complexes as Potential Cell DNA Dyes and Transfection Agents. *J. Inorg. Biochem.* **2007**, *101* (7), 1086-1089.
70. Fernandez-Moreira, V., Thorp-Greenwood, F. L., Coogan, M. P., Application of d⁶ Transition Metal Complexes in Fluorescence Cell Imaging. *Chem. Commun.* **2010**, *46* (2), 186-202.

71. Gill, M. R., Garcia-Lara, J., Foster, S. J., *et al.*, A Ruthenium(II) Polypyridyl Complex for Direct Imaging of DNA Structure in Living Cells. *Nat. Chem.* **2009**, *1* (8), 662-667.
72. Zhao, Q., Huang, C. H., Li, F. Y., Phosphorescent Heavy-Metal Complexes for Bioimaging. *Chem. Soc. Rev.* **2011**, *40* (5), 2508-2524.
73. Wilhelmsson, L. M., Westerlund, F., Lincoln, P., *et al.*, DNA-Binding of Semirigid Binuclear Ruthenium Complex $\Delta\Delta$ -[μ -(11,11'-bidppz)(phen)₄Ru₂]⁴⁺: Extremely Slow Intercalation Kinetics. *J. Am. Chem. Soc.* **2002**, *124* (41), 12092-12093.
74. Nordell, P., Lincoln, P., Mechanism of DNA Threading Intercalation of Binuclear Ru Complexes: Uni- or Bimolecular Pathways Depending on Ligand Structure and Binding Density. *J. Am. Chem. Soc.* **2005**, *127* (27), 9670-9671.
75. Westerlund, F., Nordell, P., Blechinger, J., *et al.*, Complex DNA Binding Kinetics Resolved-by Combined Circular Dichroism and Luminescence Analysis. *J. Phys. Chem B* **2008**, *112* (21), 6688-6694.
76. Westerlund, F., Nordell, P., Norden, B., *et al.*, Kinetic Characterization of an Extremely Slow DNA Binding Equilibrium. *J. Phys. Chem B* **2007**, *111* (30), 9132-9137.
77. Nordell, P., Jansson, E. T., Lincoln, P., Supercoil-Accelerated DNA Threading Intercalation. *Biochemistry* **2009**, *48* (7), 1442-1444.
78. Nordell, P., Westerlund, F., Reymer, A., *et al.*, DNA Polymorphism as an Origin of Adenine-Thymine Tract Length-Dependent Threading Intercalation Rate. *J. Am. Chem. Soc.* **2008**, *130* (44), 14651-14658.
79. Gardner, M. J., Hall, N., Fung, E., *et al.* Genome Sequence of the Human Malaria Parasite Plasmodium Falciparum. *Nature* **2002**, *419* (6906), 498-511.
80. Cantor, C. R., Schimmel, P. R., *Biophys. Chem. Part II: Techniques for the Study of Biological Structure and Function.* W. H. Freeman and Company: New York, 1980.
81. Lakowicz, J. R., *Principles of Fluorescence Spectroscopy.* 3 ed., Springer-Verlag New York Inc.: UK, 2006.
82. Kalyanasundaram, K., Photophysics, Photochemistry and Solar-Energy Conversion with Tris(bipyridyl)-Ruthenium(II) and Its Analogs. *Coord. Chem. Rev.* **1982**, *46*, 159-244.
83. Campagna, S., Puntoriero, F., Nastasi, F., *et al.*, Photochemistry and Photophysics of Coordination Compounds: Ruthenium. In *Photochem. Photophys. Coord. Compd.*, 2007, Vol. 280, 117-214.
84. Amouyal, E., Homsy, A., Chambron, J. C., *et al.*, Synthesis and Study of a Mixed-Ligand Ruthenium(II) Complex in Its Ground and Excited-States - Bis(2,2'-bipyridine)-(dipyrido[3,2-a, 2',3'-c]-phenazine-n4n5)Ruthenium(II). *J. Chem. Soc., Dalton Trans.* **1990**, (6), 1841-1845.
85. Hartshorn, R. M., Barton, J. K., Novel Dipyridophenazine Complexes of Ruthenium(II) - Exploring Luminescent Reporters of DNA. *J. Am. Chem. Soc.* **1992**, *114* (15), 5919-5925.
86. McKinley, A. W., Lincoln, P., Tuite, E. M., Environmental Effects on the Photophysics of Transition Metal Complexes with Dipyrido[3,2-a:3',2'-c]-phenazine (dppz) and Related Ligands. *Coord. Chem. Rev.* **2011**, *255* (21-22), 2676-2692.
87. Olofsson, J., Önfelt, B., Lincoln, P., Three-State Light Switch of [Ru(phen)₂dppz]²⁺: Distinct Excited-State Species with Two, One, or No Hydrogen Bonds from Solvent. *J. Phys. Chem. A* **2004**, *108* (20), 4391-4398.
88. Norden, B., Kubista, M., Kurucsev, T., Linear Dichroism Spectroscopy of Nucleic-Acids. *Q. Rev. Biophys.* **1992**, *25* (1), 51-170.

89. Nordén, B., Rodger, A., Dafforn, T., *Linear Dichroism and Circular Dichroism - a Textbook on Polarized Light Spectroscopy*. The Royal Society of Chemistry: Cambridge, 2010.
90. Wada, A., Kozawa, S., Instrument for Studies of Differential Flow Dichroism of Polymer Solutions. *J. Polym. Sci., Part A: Gen. Pap.* **1964**, 2 (2), 853-864.
91. Lincoln, P. DNA Interactions with Chiral Polyaza-Aromatic Ruthenium(II) Complexes. PhD Thesis, Chalmers University of Technology, Gothenburg, 1998.
92. Lincoln, P., Broo, A., Norden, B., Diastereomeric DNA-Binding Geometries of Intercalated Ruthenium(II) Trischelates Probed by Linear Dichroism: [Ru(phen)₂dppz]²⁺ and [Ru(phen)₂bdppz]²⁺. *J. Am. Chem. Soc.* **1996**, 118 (11), 2644-2653.
93. Lincoln, P., Norden, B., DNA Binding Geometries of Ruthenium(II) Complexes with 1,10-Phenanthroline and 2,2'-Bipyridine Ligands Studied with Linear Dichroism Spectroscopy. Borderline Cases of Intercalation. *J. Phys. Chem B* **1998**, 102 (47), 9583-9594.
94. Wilhelmsson, L. M., Esbjorner, E. K., Westerlund, F., *et al.*, Meso Stereoisomer as a Probe of Enantioselective Threading Intercalation of Semirigid Ruthenium Complex [μ-(11,11'-bidppz)(phen)₄Ru₂]⁴⁺. *J. Phys. Chem B* **2003**, 107 (42), 11784-11793.
95. Chen, F.-M., Methods for the Studies of Drug Dissociation from DNA. In: *Methods in Molecular Biology: Drug-DNA Interaction Protocols*. Fox, K. R. (Ed.), Humana Press Inc.: Totowa, New Jersey, 1998, Vol. 90, 269-274.
96. Westerlund, F., Wilhelmsson, L. M., Norden, B., *et al.*, Micelle-Sequestered Dissociation of Cationic DNA-Intercalated Drugs: Unexpected Surfactant-Induced Rate Enhancement. *J. Am. Chem. Soc.* **2003**, 125 (13), 3773-3779.
97. Li, M., Lincoln, P., Andersson, J., Slow Threading Intercalation of Monomeric Ru(II) Complexes with 10,13-Diaryl-substituted Dppz Ligands. *J. Phys. Chem B* **2011**, 115 (24), 7923-7931. (Paper III)
98. Lewis, E. A., Murphy, K. P., *Isothermal Titration Calorimetry*. In: *Methods in Molecular Biology: Protein-Ligand Interactions*. Humana Press Inc.: Totowa, New Jersey, 2005, Vol. 305.
99. Jelesarov, I., Bosshard, H. R., Isothermal Titration Calorimetry and Differential Scanning Calorimetry as Complementary Tools to Investigate the Energetics of Biomolecular Recognition. *J. Mol. Recognit.* **1999**, 12 (1), 3-18.
100. Spolar, R. S., Record, M. T., Coupling of Local Folding to Site-Specific Binding of Proteins to DNA. *Science* **1994**, 263 (5148), 777-784.
101. Ren, J. S., Jenkins, T. C., Chaires, J. B., Energetics of DNA Intercalation Reactions. *Biochemistry* **2000**, 39 (29), 8439-8447.
102. Atkins, P., de Paula, J., *Physical Chemistry*. 7th ed., Oxford University Press Inc.: New York, 2002.
103. McGhee, J. D., von Hippel, P. H., Theoretical Aspects of DNA-Protein Interactions: Co-Operative and Non-Co-Operative Binding of Large Ligands to a One-Dimensional Homogeneous Lattice. *J. Mol. Biol.* **1974**, 86, 469-489.
104. Lincoln, P., A Generalized McGhee-von Hippel Method for the Cooperative Binding of Different Competing Ligands to an Infinite One-Dimensional Lattice. *Chem. Phys. Lett.* **1998**, 288 (5-6), 647-656.
105. Pawley, J., *Handbook of Biological Confocal Microscopy*. Springer: New York, 2006.

106. Liu, F. R., Wang, K. Z., Bai, G. Y., *et al.*, The pH-Induced Emission Switching and Interesting DNA-Binding Properties of a Novel Dinuclear Ruthenium(II) Complex. *Inorganic Chemistry* **2004**, *43* (5), 1799-1806.
107. Mishra, L., Yadaw, A. K., Srivastava, S., *et al.*, Synthesis, Spectroscopic, Electrochemical and Antibacterial Studies of New Ru(II) 1,10-Phenanthroline Complexes Containing Aryldiazopentane-2,4-dione as Co-ligand *New J. Chem.* **2000**, *24* (7), 505-510.
108. Morgan, J. L., Buck, D. P., Turley, A. G., *et al.*, Meso- $[\{\text{Ru}(\text{phen})_2\}_2(\mu\text{-bpm})]^{4+}$: A High-Affinity DNA Bulge Probe. *Inorg. Chim. Acta* **2006**, *359* (3), 888-898.
109. Morgan, J. L., Buck, D. P., Turley, A. G., *et al.*, Selectivity at a Three-Base Bulge Site in the DNA Binding of $\Delta\Delta\text{-}[\{\text{Ru}(\text{phen})_2\}_2(\mu\text{-dppm})]^{4+}$. *J. Biol. Inorg. Chem.* **2006**, *11* (7), 824-834.
110. O'Reilly, F., Kelly, J., Kirsch-De Mesmaeker, A., Interaction of a Series of Bimetallic Ruthenium(II) Bipyridyl Complexes with DNA. *Chem. Commun.* **1996**, (9), 1013-1014.
111. Patterson, B. T., Collins, J. G., Foley, F. M., *et al.*, Dinuclear Ruthenium(II) Complexes as Probes for DNA Bulge Sites. *J. Chem. Soc., Dalton Trans.* **2002**, (23), 4343-4350.
112. Rajput, C., Rutkaite, R., Swanson, L., *et al.*, Dinuclear Monointercalating Ru^{II} Complexes That Display High Affinity Binding to Duplex and Quadruplex DNA. *Chem. Eur. J.* **2006**, *12* (17), 4611-4619.
113. Smith, J. A., Morgan, J. L., Turley, A. G., *et al.*, Meso- $[\{\text{Ru}(\text{phen})_2\}_2(\mu\text{-HAT})]^{4+}$: A High-Affinity DNA Hairpin Probe. *Dalton Trans.* **2006**, (26), 3179-3187.
114. Wu, J. Z., Yuan, L., Synthesis and DNA Interaction Studies of a Binuclear Ruthenium(II) Complex with 2,9-bis(2-imidazo[4,5-f][1,10]phenanthroline)-1,10-phenanthroline as Bridging and Intercalating Ligand. *J. Inorg. Biochem.* **2004**, *98* (1), 41-45.
115. Zou, X. H., Ye, B. H., Li, H., *et al.*, Mono- and Binuclear Ruthenium(II) Complexes Containing a New Asymmetric Ligand 3-(pyrazin-2-yl)-as-triazino[5,6-f]1,10-phenanthroline: Synthesis, Characterization and DNA-Binding Properties. *J. Chem. Soc., Dalton Trans.* **1999**, (9), 1423-1428.
116. O'Reilly, F. M., Kelly, J. M., Binding of Bimetallic 1,10-Phenanthroline Ruthenium(II) Complexes to DNA. *New J. Chem.* **1998**, *22* (3), 215-217.
117. Westerlund, F., Eng, M. P., Winters, M. U., *et al.*, Binding Geometry and Photo-physical Properties of DNA-Threading Binuclear Ruthenium Complexes. *J. Phys. Chem B* **2007**, *111* (1), 310-317.
118. Chitrapriya, N., Jang, Y. J., Kim, S. K., *et al.*, Non-Intercalative Binding Mode of Bridged Binuclear Chiral Ru(II) Complexes to Native Duplex DNA. *J. Inorg. Biochem.* **2011**, *105* (12), 1569-1575.
119. Li, M., Lincoln, P., Synthesis and DNA Threading Properties of Quaternary Ammonium $[\text{Ru}(\text{phen})_2(\text{dppz})]^{2+}$ Derivatives. *J. Inorg. Biochem.* **2009**, *103* (7), 963-970.
120. Grimm, G. N., Boutorine, A. S., Lincoln, P., *et al.*, Formation of DNA Triple Helices by an Oligonucleotide Conjugated to a Fluorescent Ruthenium Complex. *ChemBioChem* **2002**, *3* (4), 324-331.
121. Tuite, E., Lincoln, P., Norden, B., Photophysical Evidence That $\Delta\text{-}$ and $\Lambda\text{-}$ $[\text{Ru}(\text{phen})_2(\text{dppz})]^{2+}$ Intercalate DNA from the Minor Groove. *J. Am. Chem. Soc.* **1997**, *119* (1), 239-240.

122. Dupureur, C. M., Barton, J. K., Use of Selective Deuteration and $^1\text{H-NMR}$ in Demonstrating Major Groove Binding of Δ - $[\text{Ru}(\text{phen})_2\text{dppz}]^{2+}$ to $d(\text{GTCGAC})_2$. *J. Am. Chem. Soc.* **1994**, *116* (22), 10286-10287.
123. Dupureur, C. M., Barton, J. K., Structural Studies of Λ - and Δ - $[\text{Ru}(\text{phen})_2\text{dppz}]^{2+}$ Bound to $d(\text{GTCGAC})_2$: Characterization of Enantioselective Intercalation. *Inorg. Chem.* **1997**, *36* (1), 33-43.
124. Jenkins, Y., Friedman, A. E., Turro, N. J., *et al.*, Characterization of Dipyridophenazine Complexes of Ruthenium(II) - the Light Switch Effect as a Function of Nucleic-Acid Sequence and Conformation. *Biochemistry* **1992**, *31* (44), 10809-10816.
125. Turro, C., Bossmann, S. H., Jenkins, Y., *et al.*, Proton-Transfer Quenching of the MLCT Excited-State of $\text{Ru}(\text{phen})_2\text{dppz}^{2+}$ in Homogeneous Solution and Bound to DNA. *J. Am. Chem. Soc.* **1995**, *117* (35), 9026-9032.
126. Haq, I., Lincoln, P., Suh, D. C., *et al.*, Interaction of Δ - $[\text{Ru}(\text{phen})_2\text{dppz}]^{2+}$ and Λ - $[\text{Ru}(\text{phen})_2\text{dppz}]^{2+}$ with DNA - a Calorimetric and Equilibrium Binding Study. *J. Am. Chem. Soc.* **1995**, *117* (17), 4788-4796.
127. Önfelt, B., Göstring, L., Lincoln, P., *et al.*, Cell Studies of the DNA Bis-Intercalator $\Delta\Delta$ - $[\mu\text{-C4}(\text{cpdppz})_2\text{-(phen)}_4\text{Ru}_2]^{4+}$: Toxic Effects and Properties as a Light Emitting DNA Probe in V79 Chinese Hamster Cells. *Mutagenesis* **2002**, *17* (4), 317-320.
128. Pisani, M. J., Fromm, P. D., Mulyana, Y., *et al.*, Mechanism of Cytotoxicity and Cellular Uptake of Lipophilic Inert Dinuclear Polypyridyl Ruthenium(II) Complexes. *ChemMedChem* **2011**, *6* (5), 848-858.
129. Pisani, M. J., Weber, D. K., Heimann, K., *et al.*, Selective Mitochondrial Accumulation of Cytotoxic Dinuclear Polypyridyl Ruthenium(II) Complexes. *Metallomics* **2010**, *2* (6), 393-396.
130. Ossipov, D., Pradeepkumar, P. I., Holmer, M., *et al.*, Synthesis of $[\text{Ru}(\text{phen})_2\text{dppz}]^{2+}$ -Tethered Oligo-DNA and Studies on the Metallointercalation Mode into the DNA Duplex. *J. Am. Chem. Soc.* **2001**, *123* (15), 3551-3562.
131. Puckett, C. A., Barton, J. K., Fluorescein Redirects a Ruthenium-Octaarginine Conjugate to the Nucleus. *J. Am. Chem. Soc.* **2009**, *131* (25), 8738-8739.
132. Puckett, C. A., Barton, J. K., Targeting a Ruthenium Complex to the Nucleus with Short Peptides. *Bioorg. Med. Chem.* **2010**, *18* (10), 3564-3569.
133. Jenkins, Y., Barton, J. K., A Sequence-Specific Molecular Light Switch - Tethering of an Oligonucleotide to a Dipyridophenazine Complex of Ruthenium(II). *J. Am. Chem. Soc.* **1992**, *114* (22), 8736-8738.
134. Puckett, C. A., Barton, J. K., Methods to Explore Cellular Uptake of Ruthenium Complexes. *J. Am. Chem. Soc.* **2007**, *129* (1), 46-47.
135. Puckett, C. A., Barton, J. K., Mechanism of Cellular Uptake of a Ruthenium Polypyridyl Complex. *Biochemistry* **2008**, *47* (45), 11711-11716.
136. Svensson, F. R., Matson, M., Li, M., *et al.*, Lipophilic Ruthenium Complexes with Tuned Cell Membrane Affinity and Photoactivated Uptake. *Biophys. Chem.* **2010**, *149* (3), 102-106.